








Article

NGIWY-Amide: A Bioinspired Ultrashort Self-Assembled Peptide Gelator for Local Drug Delivery Applications

Nikoleta F. Theodoroula ¹, Christina Karavasili ², Manos C. Vlasίου ³, Alexandra Primikyri ⁴,
Christia Nicolaou ³, Alexandra V. Chatzikonstantinou ⁵, Aikaterini-Theodora Chatzitaki ², Christos Petrou ³,
Nikolaos Bouropoulos ^{6,7}, Constantinos K. Zacharis ⁸, Eleftheria Galatou ³, Yiannis Sarigiannis ^{3,*},
Dimitrios G. Fatouros ² and Ioannis S. Vizirianakis ^{1,3,*}

- ¹ Department of Molecular Pharmacology, School of Pharmacy, Aristotle University of Thessaloniki, 54124 Thessaloniki, Greece; theodorn@pharm.auth.gr
- ² Department of Pharmaceutical Technology, School of Pharmacy, Aristotle University of Thessaloniki, 54124 Thessaloniki, Greece; karavasc@pharm.auth.gr (C.K.); chatzita@pharm.auth.gr (A.-T.C.); dfatouro@pharm.auth.gr (D.G.F.)
- ³ Department of Life & Health Sciences, University of Nicosia, Nicosia 2417, Cyprus; vlasiou.m@unic.ac.cy (M.C.V.); krinikolaou@gmail.com (C.N.); petrou.c@unic.ac.cy (C.P.); galatou.e@unic.ac.cy (E.G.)
- ⁴ Department of Chemistry, University of Ioannina, 45110 Ioannina, Greece; a.primikyri@uoi.gr
- ⁵ Biotechnology Laboratory, Department of Biological Applications and Technologies, University of Ioannina, 45110 Ioannina, Greece; achatzikonstantinou@uoi.gr
- ⁶ Department of Materials Science, University of Patras, 26504 Patras, Greece; nbouro@upatras.gr
- ⁷ Foundation for Research and Technology Hellas, Institute of Chemical Engineering and High Temperature Chemical Processes, 26504 Patras, Greece
- ⁸ Laboratory of Pharmaceutical Analysis, Department of Pharmaceutical Technology, School of Pharmacy, Aristotle University of Thessaloniki, 54124 Thessaloniki, Greece; czacharis@pharm.auth.gr
- * Correspondence: sarigiannis.i@unic.ac.cy (Y.S.); ivizir@pharm.auth.gr (I.S.V.)



Citation: Theodoroula, N.F.; Karavasili, C.; Vlasίου, M.C.; Primikyri, A.; Nicolaou, C.; Chatzikonstantinou, A.V.; Chatzitaki, A.-T.; Petrou, C.; Bouropoulos, N.; Zacharis, C.K.; et al. NGIWY-Amide: A Bioinspired Ultrashort Self-Assembled Peptide Gelator for Local Drug Delivery Applications. *Pharmaceutics* **2022**, *14*, 133. <https://doi.org/10.3390/pharmaceutics14010133>

Academic Editor: Rakesh Tiwari

Received: 11 December 2021

Accepted: 31 December 2021

Published: 6 January 2022

Publisher's Note: MDPI stays neutral with regard to jurisdictional claims in published maps and institutional affiliations.



Copyright: © 2022 by the authors. Licensee MDPI, Basel, Switzerland. This article is an open access article distributed under the terms and conditions of the Creative Commons Attribution (CC BY) license (<https://creativecommons.org/licenses/by/4.0/>).

Abstract: Fibrillar structures derived from plant or animal origin have long been a source of inspiration for the design of new biomaterials. The Asn-Gly-Ile-Trp-Tyr-NH₂ (NGIWY-amide) pentapeptide, isolated from the sea cucumber *Apostichopus japonicus*, which spontaneously self-assembles in water to form hydrogel, pertains to this category. In this study, we evaluated this ultra-short cosmetic bioinspired peptide as vector for local drug delivery applications. Combining nuclear magnetic resonance, circular dichroism, infrared spectroscopy, X-ray diffraction, and rheological studies, the synthesized pentapeptide formed a stiff hydrogel with a high β -sheet content. Molecular dynamic simulations aligned well with scanning electron and atomic-force microscopy studies, revealing a highly filamentous structure with the fibers adopting a helical-twisted morphology. Model dye localization within the supramolecular hydrogel provided insights on the preferential distribution of hydrophobic and hydrophilic compounds in the hydrogel network. That was further depicted in the diffusion kinetics of drugs differing in their aqueous solubility and molecular weight, namely, doxorubicin hydrochloride, curcumin, and octreotide acetate, highlighting its versatility as a delivery vector of both hydrophobic and hydrophilic compounds of different molecular weight. Along with the observed cytocompatibility of the hydrogel, the NGIWY-amide pentapeptide may offer new approaches for cell growth, drug delivery, and 3D bioprinting tissue-engineering applications.

Keywords: ultra-short peptides; smart materials; NGIWY-amide; self-assembled peptide hydrogels; drug delivery; sea cucumber

1. Introduction

Ultra-short peptide hydrogels, with two to seven amino acids, have gained the interest of scientists due to their involvement in important biological processes [1]. In addition to their advances in therapeutics [2], they are used in advanced nano-supramolecular

technologies [3], novel smart bio-functional materials [4], vaccines [5], delivery systems for small drugs [6], biologics [7], and genes [8], as well as for cosmetics [9]. Furthermore, ultra-short peptide hydrogels, due to the ease of synthesis and scaling up, feasibility to modifications [10], non-immunogenicity, non-genotoxicity, biocompatibility and biodegradability, and mechanical stability [11], are widely used as starting materials for bioimaging probes [12], 3D bioprinting ink [13,14], and cell culture scaffolds for organoids [15]. Hydrogelation is mediated through hydrogen bonding, van der Waals forces, or π - π stacking of aromatic groups that drive the formation of nanofibrillar structures that further interweave into α -helices, β -sheets, hairpins, turns, micelles, ribbons, tapes, tubes, and coils [16,17]. Fibrillar structures are key elements in biological systems since they have been identified in both physiological (blood coagulation) and pathological conditions (interestingly, in degenerative diseases, e.g., Parkinson's, Alzheimer's) [18].

Drawing structures from nature to generate high-performance soft materials is a promising approach for the construction of functional biomaterials with advanced properties, like facilitating the transport processes inside organisms and molecular recognition. These moieties not only exhibit enhanced bioavailability but also act as "self-delivery" systems without involving other natural or artificial materials (hyaluronic acid, chitosan, etc). Moreover, light backbone and side-chain modifications of biomolecules in a cost-effective manner offer the essential fine-tuning in the structures to fabricate biofunctional materials with often-enticing chemical, physical, mechanical, and biological properties, ideal for a wide range of applications [19].

NGIWY-amide (Asn-Gly-Ile-Trp-Tyr-NH₂) (Figure 1) is among the few known neuropeptides isolated from echinoderms, in particular from the sea cucumber *Apostichopus japonicus* [20]. Localized in the holothurian nervous system, the peptide stiffens the dermis of the sea cucumber body wall. Dermis is a catch connective tissue, and its mechanical properties are modulated in response to other neuropeptides, like holokinins. Apart from its contractile action, the pentapeptide has been assessed for its gonadotropic action, as it induces oocyte maturation and gamete spawning of *A. japonicus* [21]. Compounds isolated from sea cucumbers are under extensive investigations applied in the cosmetic industry [22].

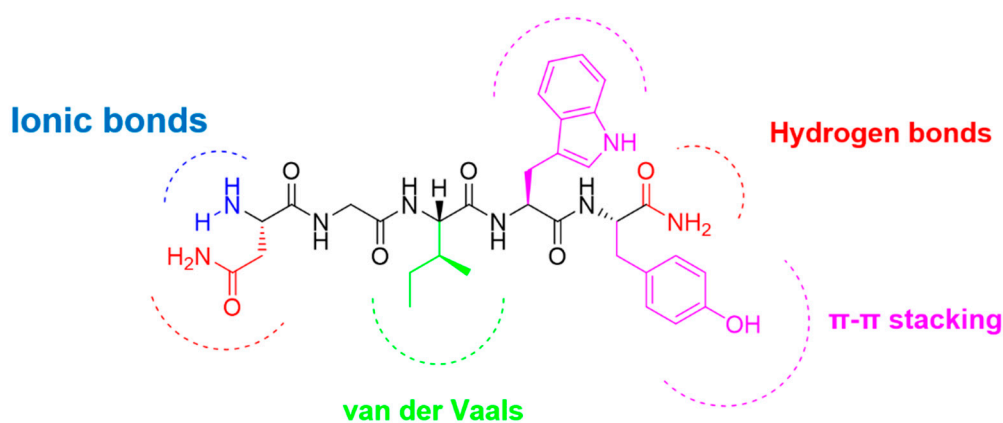


Figure 1. The structure of the pentapeptide NGIWY-amide.

The balance between hydrophilicity and hydrophobicity can positively contribute to adequate gelation properties. The pentapeptide consists of two hydrophilic amino acids (N: Asn, G: Gly) at the N-terminal site and three hydrophobic amino acids at the C-terminal site, forming a small amphiphile. The backbone over-satisfies the criteria for gelling [10]. Naturally occurring aromatic amino acids Phe, Tyr, Trp, and even His form well-ordered nanostructures like fibrils, ribbons, or rods [23]. Two aromatic amino acids, tryptophan and tyrosine, are incorporated into the sequence and involved in intra- and intermolecular interactions due to the π - π stacking of the aromatic rings of the side chains. The backbone conformation of the peptide sequence is also responsible for its molecular

self-assembly and mechanical stiffness. Glycine is among the amino acids that usually participate in the nanofiber's formation. Isoleucine, an aliphatic amino acid, favors van der Waals forces and asparagine due to the side-chain carboxamide group inducing hydrogen bonds completing the most important interactions in peptide self-assembly. Hydrogen-bond formation, determining the secondary structure of the peptides, is also assisted by the C-terminal carboxamide. The peptide has a positive net charge of +1 due to the free amino group at the N-terminal site. The synergism and cooperativeness of all these weak interactions lead to a dynamic and responsive interplay around the peptide structure, leading to a functional material when it is exposed in an aqueous environment.

Yet, there is no study evaluating the ability of NGIWY-amide to self-assemble or its potential as a platform technology for local drug delivery or other similar applications. The self-assembling pentapeptide was studied *in silico* by using molecular dynamics (MD) simulations, and after the synthesis, the formed hydrogel was characterized and studied with nuclear magnetic resonance (NMR) for the inter- and intramolecular interactions of the peptide with the aqueous environment. Furthermore, an array of techniques, namely, atomic force microscopy (AFM) and transmission electron microscopy (TEM), Fourier transform-infrared spectroscopy (FT-IR) and X-ray diffraction (XRD), oscillatory rheology, UV/Vis, and fluorescence, were enrolled for the assessment of the peptide. Circular dichroism (CD) studies were used to obtain the essential information for the secondary structure of the peptide hydrogel. Confocal laser scanning microscopy (CLSM) was conducted for the localization of two model fluorescent dyes within the pentapeptide hydrogel. *In vitro* release studies and kinetic analysis were also performed, and cell culture-based biological assays were applied to certify the biocompatibility of the hydrogel.

2. Materials and Methods

2.1. Materials

Common solvents and reagents used in solid-phase peptide synthesis were purchased from commercial suppliers (Sigma-Aldrich, Merck-Millipore, etc.) and used without further purification unless otherwise noted. Rink Amide MBHA resin and Fmoc-protected amino acids were purchased from CBL Patras (Patras, Greece). ChemMatrix-Rink Amide resin was also purchased from Biotage (Uppsala, Sweden). Hydrochloric acid (HCl) (36.5–38%) was obtained from EM Industries, and acetic acid (AcOH) (99–100%) and ammonium hydroxide (NH₄OH) (25%) were purchased from VWR Chemicals. Sodium deuterioxide (NaOD) (30% *w/v*, 99.5% D) and deuterium oxide (D₂O) (99.9% D) were purchased from Cambridge Isotope Laboratories. Nile blue A, calcein, doxorubicin hydrochloride (98.0–102.0% HPLC), curcumin (from *Curcuma longa*), and trifluoroacetic acid (99%) were purchased from Sigma-Aldrich (Darmstadt, Germany). Acetonitrile (HPLC grade) was obtained from VWR Chemicals (Vienna, Austria). A B30 water purification system (Adrona SIA, Riga, Latvia) was utilized. Octreotide acetate was kindly gifted from Pharmathen (Athens, Greece). Milli-Q water was used in all studies.

2.2. Peptide Synthesis

The peptide was synthesized by using microwave-assisted solid-phase peptide synthesis on a single-channel microwave peptide synthesizer (Biotage[®] Initiator+ SP Wave, Biotage, Sweden), standard Fmoc protection, and DIC/Oxyma pure activation strategies. Briefly, 0.3 g Rink Amide MBHA resin (100–200 mesh, 0.71 mmol g⁻¹, CBL Patras, Greece) or H-Rink Amide ChemMatrix[®] resin (100–200 mesh, 0.45 mmol g⁻¹, Biotage, Sweden) were used to provide C-terminal peptide amides after the final cleavage from the solid support. The resin was swollen in *N,N*-dimethylformamide (DMF) at room temperature for 15 min under agitation (1200 rpm). The Fmoc protecting group was removed from the capped amino group by treatment of the resin with 2% DBU and 5% piperazine in DMF within 1 min at 90 °C under microwave irradiation. Couplings were performed under microwave irradiation for 5 min at 75 °C with 3.0 eq. of the required Fmoc amino acid, 3.3 eq. of *N,N*-diisopropylcarbodiimide (DIC), and 4.5 eq. of Oxyma pure as activator in

DMF. After each deprotection step and coupling, a Kaiser test was performed to ensure completion of the reaction. After the completion of the synthesis, the resin was treated with a mixture of trifluoroacetic acid (TFA), triisopropylsilane (TIS), and water (95:2.5:2.5, *v/v*) (10 mL cleavage solution/g dry peptide–resin) at room temperature for 2.5 h to cleave the peptide from the resin as well as to remove the side-chain protection groups. The solution was filtered off and the solvent mixture was removed *under vacuo* and the white off peptide was recovered in chilled diethyl ether, then centrifuged to obtain the peptide precipitate, dissolved in water, and freeze-dried for 48 h.

2.3. Characterization with Liquid Chromatography–Mass Spectroscopy (LC-MS) and Nuclear Magnetic Resonance (NMR)

The lyophilized crude peptide was analyzed for its purity (~92%) with high-performance liquid chromatography (Alliance HPLC e2695, PDA 2998, Waters, Milford, MA, USA) and electrospray ionization mass spectrometry (ACQUITY QDa Mass Detector, Waters, Milford, MA, USA). The peptide was eluted at 10.79 min through Hypersil Gold (100 × 2.1 mm, 3 μm) at a flow of 0.3 mL/min with a linear gradient system (5 to 100% B) for 30 min (A: 0.1% TFA in H₂O, B: 0.1% TFA in MeCN (Figure S1)). The observed mass of the main peak corresponds to the $[M + H]^+ = 651.36$ and the peak at $[M + Na]^+ = 673.45$. ¹H and ¹³C NMR spectra experiments were obtained in D₂O on a Bruker AV500 spectrometer (Bruker Biospin, Rheinstetten, Germany) at 298 K using the Topspin 3.2 suite. Samples (0.5 mg) of the peptide were dissolved in 0.6 mL of deuterated water and transferred to 5 mm NMR tubes. Water suppression in the 1D ¹H NMR and the 2D ¹H-¹H NOESY spectra was achieved using an excitation-sculpting pulse sequence. The mixing time in the 2D ¹H-¹H NOESY spectrum was set to 600 ms to obtain the maximum intensity. The 2D ¹H-¹³C HSQC and ¹H-¹³C HMBC NMR experiments were recorded using standard Bruker software (Table S1).

The peptide hydrogel (1% *w/v*, 15.3 mM) was prepared in the tube (600 μL of D₂O hot solution were transferred into the NMR tube and allowed to cool down and gelate inside the tube). By using excitation sculpting for water suppression (zgpg30) with a recycle delay of 10 s, ¹H NMR spectra were acquired. In the 2D ¹H-¹H NOESY spectrum, the mixing time of the hydrogel was set to 300 ms. Saturation transfer difference (STD) NMR experiments were performed with the selective saturation of a given ¹H frequency by a train of 40 Gaussian pulses with a duration of 50 ms each, separated by a delay of 1 ms. The on-resonance irradiation was performed at a saturation frequency of −0.6 ppm, where only resonances of the hydrogel network can be encountered. Off-resonance irradiation was applied at 40 ppm, outside the spectra region of the ¹H NMR resonances. The saturation time was set to 2 s. The STD spectrum was created by the subtraction of the on-resonance spectrum from the off-resonance spectrum.

2.4. Molecular Dynamics Simulations and Density Functional Theory Study

Avogadro software with the peptide-builder tool was used to create the peptide NGIWY peptide. Using the Assisted Model Building with Energy Recruitment (AMBER) 94 forcefield, a custom script was used to amidate the C-termini in VMD3. Proteins and nucleic acids were parameterized specifically. Only bonding and non-bonding terminology are used in AMBER, as well as a complex electrostatic treatment. For proteins, nucleic acids, and peptides, the results are excellent, but for other systems, such as bioinorganic and bioorganic systems, the results can be inconsistent. The simulations were run in NAMD 2.105 with final production trajectories of 200 ns. Scripts built in the Python6 programming language, as well as VMD, were used to process and further analyze trajectory data. The SURF computation (surface areas) was used to characterize the peptide structure, with the solvent probe radius set to 1.4 for any and all peptides. Clusters were established within 1.4 Å of each other in this way. The Kyte–Doolittle (KD) hydrophobicity indices were averaged over the amino acid sequence to obtain grand average hydropathicity (GRAVY) values. The optimized PM3 structures were used to distribute density functional theory

calculations, with the ORCA program used to calculate the quantum mechanical descriptors associated with reactivity. DFT was used to perform geometry optimizations and frequency computations in the aqueous phase, utilizing the functional B3LYP, which could be a hybrid Hartree–Fock density functional theory (HF-DFT).

2.5. Molecular Docking Study

The docking study was performed for the target peptide on the albumin using the AutoDock4 software. During this study, the crystallized protein located at the Protein Data Bank (PDB, <https://www.rcsb.org/>; last accessed 12 November 2021) was used. The water molecules co-crystallized with HSA structures were removed for the docking investigations, and the peptide recognition site was determined using residues within a grid of $60 \text{ \AA} \times 60 \text{ \AA} \times 60 \text{ \AA}$, with a population of 100 randomly arranged individuals and a maximum number of 1.0×10^7 energy assessments. Prior to docking, the target peptide was drawn within the Chem3D Pro and Chimera software, and the peptides were subjected to minimization energy using the hybrid functional B3LYP with a 6-311G (d, p) basis set. The conformation with the lowest free energy values of the peptide linked on HSA protein was used to calculate the ΔG (kcal/mol) of the peptide structure. Chimera software was used to create the figures for the protein and the peptide.

2.6. Peptide Supramolecular Hydrogel Formation and Characterization

To analyze the gelation behavior, gelation kinetics and the hydrogel's viscoelastic properties were monitored on a Physica MCR 300 rheometer (Physica Messtechnik GmbH, Stuttgart, Germany) with cone-plate geometry (diameter 25 mm, cone angle 1° , gap 0.05 mm). The temperature was regulated at $25 \pm 0.1^\circ \text{C}$ using a Paar Physica circulating bath and a controlled Peltier system (TEZ 150P/MCR). Oscillatory time-sweep experiments were performed at a frequency of 1 Hz and a strain of 0.1%, followed by frequency-sweep tests in the frequency range of 0.01–100 Hz and at a strain of 0.1%. Prior to the measurements, fresh peptide hydrogels were prepared in Milli-Q water at final concentrations of 2%. NGIWY-amide pentapeptide was dissolved in Milli-Q water, vortexed for 1 min, and further sonicated (Sonorex Digitec, Bandelin, Germany) at 25°C for 10 min until a clear solution was obtained.

FT-IR was performed to monitor the interactions in the amide I region ($1550\text{--}1750 \text{ cm}^{-1}$) using an IR Prestige-21 (Shimadzu). The FTIR spectrum in a wavenumber ranging between 4000 and 800 cm^{-1} was acquired in a sample of freeze-dried pentapeptide hydrogel (2% *w/v*). The crystallinity of the freeze-dried pentapeptide hydrogel was characterized via Bruker D8-Advance diffractometer with $\text{CuK}\alpha$ radiation (after gold coating) and the spectrum was recorded at 2θ from 10° to 60° . Freshly prepared peptide hydrogel samples (0.02% *w/v*) were used to record the UV-Vis and fluorescence absorbance spectra. The fluorescence emission spectrum (RF-5301 fluorophotometer, Shimadzu) was obtained over a range of 290–550 nm with excitation and emission slit widths set to 5 nm and 1.5 nm, respectively, and at an excitation of 280 nm. The UV-vis spectrum was recorded in the wavelength range of 200–800 nm on a UV-2501 spectrometer (Shimadzu). Circular dichroism experiments were carried out in double-distilled water using a Jasco J-1500 spectropolarimeter (Tokyo, Japan) equipped with a Peltier system for temperature control. Acquisitions were performed at 25°C , between 190 and 260 nm with a 0.1 nm data pitch, 1 nm bandwidth, 100 nm/min scanning speed, and 1 s response time when a 0.1 cm quartz cuvette was used. When a 1 cm quartz cuvette was used, the acquisitions were performed at 25°C between 190 nm and 260 nm with a 1 nm data pitch, 1 nm bandwidth, 500 nm/min scanning speed, and 1 s response time. All the spectra were acquired as an average of 3 scans and were corrected from a double-distilled water reference solution. The results were analyzed using Jasco Spectra Manager software.

2.7. Morphological Assessment

The hydrogel microstructure was visualized with atomic force microscopy (AFM) using a Veeco Multimode AFM (Veeco Instruments, Inc., Santa Barbara, CA, USA) with a Nanoscope IIIa controller. A 10 μL drop of the pentapeptide hydrogel (2% *w/v*) was transferred by pipetting onto a mica surface. After 30 s, the mica was rinsed with 300 μL Milli-Q water and air-dried. The height images were acquired using cantilevers with a spring constant of 10 N/m while the scan rate was adjusted to 1 Hz.

For transmission electron microscopy (TEM) visualization of the peptide hydrogel (2% *w/v*), an aliquot of 10 μL was deposited on carbon film-coated grids and air-dried prior imaging with TEM Jeol 2100 operated at 200 kV. ImageJ software was used to determine the mean fiber diameter by randomly measuring 100 fibers from the TEM images.

2.8. Confocal Laser-Scanning Microscopy (CLSM) and In Vitro Drug Release Studies and Kinetics

Localization of two model fluorescent dyes, namely, Nile blue (lipophilic) and calcein (hydrophilic), within the pentapeptide hydrogel microstructure was assessed with confocal laser-scanning microscopy. Two microliters of Nile blue (100 $\mu\text{g}/\text{mL}$ in ethanol) or calcein (400 $\mu\text{g}/\text{mL}$ in water) were loaded into 20 μL of the peptide hydrogel (2% *w/v*). Samples were imaged with a 63 \times oil-immersion lens under a Zeiss LSM 780 CLSM (Carl Zeiss Microscopy GmbH, Berlin, Germany) using appropriate filters. Images were obtained using ZEN 2011 software.

The in vitro release profiles of octreotide acetate, doxorubicin hydrochloride, and curcumin from the pentapeptide hydrogel (2% *w/v*) were recorded in phosphate-buffered saline (PBS, pH 7.4) at 37 $^{\circ}\text{C}$, whereas in the case of curcumin, Tween 80 (0.1% *v/v*) was added in the medium to assure sink conditions. The drug-loaded pentapeptide hydrogels were prepared at a final drug concentration of 0.5 mg/mL for octreotide acetate and doxorubicin hydrochloride and at 0.2 mg/mL for curcumin. Release studies were conducted in Eppendorf tubes, in which the drug-loaded hydrogels (50 μL) were left overnight at RT, prior to the gentle addition of 1 mL release medium on top of them. At predetermined time-points, samples (800 μL) were collected and replaced by an equal amount of fresh and prewarmed medium. HPLC analysis was performed for the quantification of octreotide acetate, whereas doxorubicin and curcumin were quantified by fluorescence spectroscopy. Excitation and emission wavelengths were set to 488 nm and 590 nm, respectively, for doxorubicin hydrochloride (excitation/emission slit widths: 5 nm/10 nm) and at 420 nm and 550 nm for curcumin (excitation/emission slit widths: 5 nm/10 nm). The release kinetics of all drugs from the peptide hydrogel were analyzed according to different mathematical models (zero order, first order, Korsmeyer–Peppas, Higuchi, Hixon–Crowell, and Weibull) using the excel add-in software DDSolver. For the analysis of octreotide acetate, an HPLC method was developed and validated in-house. HPLC instrumentation (Shimadzu, Kyoto, Japan) consisted of two LC-20AD isocratic high-performance pumps, an autosampler (SIL-20C HT), a column oven (CTO-20AC), and a photo-diode array detector (SPD-M20A). LabSolutions software (vs. 5.42SP3) was utilized for HPLC instrument control and operation. The separation of octreotide from the sample matrix was performed using a Nucleodur C18 analytical column (125 \times 4.6 mm, 5 μm) (Macherey-Nagel, Germany). The column oven was set to 30 $^{\circ}\text{C}$. The mobile phases were water (mobile phase A) and acetonitrile (mobile phase B), both containing 0.1% *v/v* trifluoroacetic acid. A binary gradient elution was used, starting from 5% *v/v* B and followed by a linear increase to 50% *v/v* B in 6 min. Then it was kept constant for up to one minute and altered to 5% B at 8 min. Then, the column was equilibrated for 15 min (at the initial conditions) in order to obtain reproducible retention times. A volume of 20 μL was injected to the column while the flow rate was set to 1 mL min^{-1} . The octreotide was monitored at 210 nm. The processed samples were kept at 10 $^{\circ}\text{C}$ in the autosampler tray prior to analysis. A washing mixture of 50/50% *v/v* $\text{H}_2\text{O}/\text{CH}_3\text{OH}$ was employed between analyses in order to avoid potential carryover.

Using the above conditions, the octreotide peak was well resolved from the matrix, with a retention time of 11 min. The linearity of the HPLC method was investigated in the range of 0.5–50 $\mu\text{g}/\text{mL}$ with $R^2 = 0.9982$ using 7 calibrants prepared in water. The limit of quantitation (LOQ) was 0.5 $\mu\text{g}/\text{mL}^{-1}$ and the % RSD was less than 1.0% ($n = 3$).

2.9. *In Vitro* Cell Viability and Cell Death Assays

The cell lines MRC5 (normal) and HSC3 (malignant) were grown in culture in Dulbecco's Modified Eagle Medium (DMEM) supplemented with 10% (*v/v*) fetal bovine serum (FBS) and containing 1% *v/v* penicillin–streptomycin solution. The incubation of cells was at 37 °C in a humidified atmosphere with 5% *v/v* CO₂. Before each experiment, the cells were washed with phosphate-buffered saline (PBS) pH 7.4 and then were harvested by trypsinization and centrifuged at 1000 rpm for 5 min. After resuspension, 5×10^3 cells were seeded per well in a 96-well plate and incubated as mentioned above. The following day, various amounts of the NGIWY amide peptide (0, 0.01, 0.1, 0.2, 0.4, 0.6 mg/mL) were separately added in cultures to assess cell viability. Five independent biological experiments were conducted for the measurement of cell viability for each concentration and all data presented are the average from triplicate experiments. After 24, 48, and 72 h of incubation. Cell Counting Kit-8 (CCK8, St. Louis, MO, Sigma-Aldrich) reagent was added to each well, and after incubation for 2 h at 37 °C, the OD was assessed at 450 nm in a multifunction microplate reader. Wells containing only the CCK-8 reagent were used as blank control.

Complementary to cell viability assessment, the number of dead cells in cultures exposed to various concentrations of the NGIWY amide peptide (0, 0.01, 0.1, 0.2, 0.4, 0.6 mg/mL) mentioned above was also determined using the trypan blue exclusion method, as previously described [24].

2.10. Statistical Analysis

Data are presented as mean \pm standard deviation (SD) of triplicate incubations. Statistical analysis was performed using one-way analysis of variance (ANOVA) and significance level was set at $p < 0.05$.

3. Results

3.1. Synthesis and Characterization of the Self-Assembled Pentapeptide

NGIWY-amide high-performance liquid chromatography and electrospray ionization mass spectrometry (LC-PDA-ESI-MS) revealed the high purity of the peptide and the expected molecular mass of 650.36, as shown in Figures S1 and S2, respectively. Analytical data of the NMR experiments, ¹H and ¹³C NMR spectra obtained in D₂O, are displayed in Table S1 of the Supporting Information.

3.2. NMR Studies

3.2.1. ¹H NMR of the Peptide Hydrogel

The extent of the gelator molecule incorporation into the hydrogel network was assessed with 1D ¹H NMR spectroscopy, since these molecules do not become observable with solution-state NMR spectroscopy. Changes in the peak intensities, linewidths, and chemical shifts allow for the evaluation of the ratio between the free molecules in the isotropic phase and the molecules forming the hydrogel fibers [25]. All sharp and intense ¹H NMR peaks of the NGIWY peptide in solution were broader and less intense in the ¹H NMR spectrum of the NGIWY hydrogel since all the peaks of the peptide reflected the state in the hydrogel form (Figure 2A,B). The linewidth was further increased, and broadening reached a plateau 24,332 h after the gel preparation (Figure 2C). Approximately 50% of gelator molecules became structural components of the hydrogel fibers. However, the exact percentage of the incorporation is highly dependent on the time of the acquisition of the initial spectrum and on the kinetics of the gelation due to factors such as temperature.

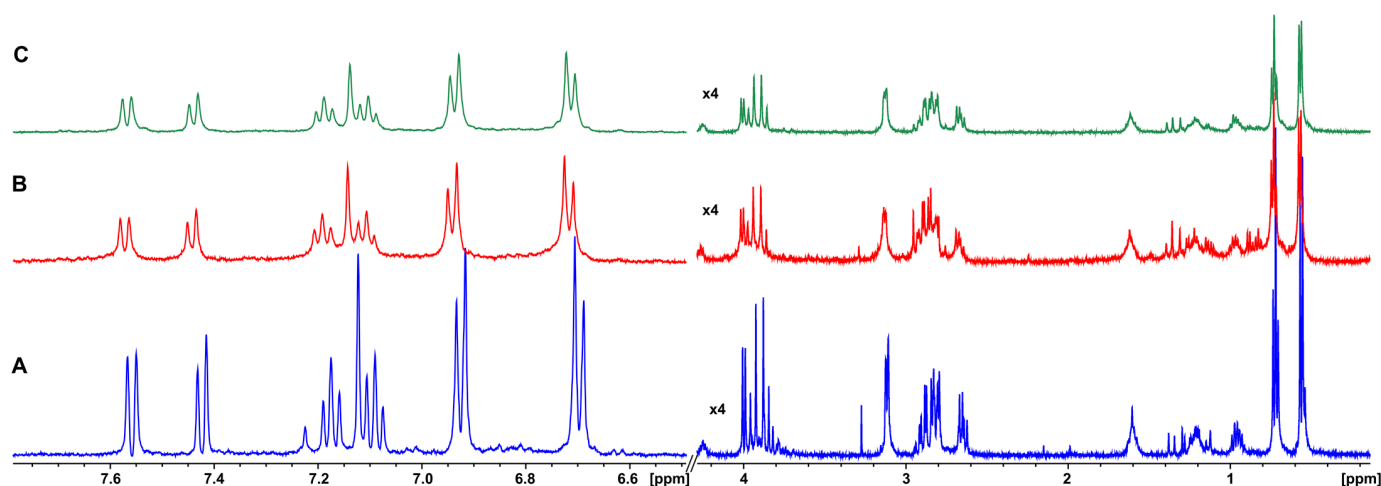


Figure 2. (A) ^1H NMR spectrum of NGIWY (1.3 mM) peptide in solution (500 MHz, PBS in D_2O pH 7.4). (B) ^1H NMR spectrum of NGIWY (1% *w/v*, 15.3 mM) (500 MHz, PBS in D_2O pH 7.4) ~10 min after the initial preparation. (C) ^1H NMR spectrum of NGIWY (1% *w/v*, 15.3 mM) (500 MHz, PBS in D_2O pH 7.4) 24 h after the initial preparation.

3.2.2. NOESY NMR of the Peptide Hydrogel

A ^1H - ^1H NOESY (nuclear Overhauser effect spectroscopy) spectrum was recorded for the NGIWY peptide in the soluble form at a concentration of 1.3×10^{-3} M. The NOESY spectrum showed several well-resolved weak positive NOEs (cross-peaks with opposite sign with respect to the diagonal), as expected for a low-molecular-weight molecule (Figure 3). The intermolecular interactions responsible for the formation of the hydrogel network were then investigated and in the 2D NOESY spectrum of the hydrogel, strong negative NOE enhancements appeared. This effect is characteristic for large-molecular-weight molecules that transfer magnetization efficiently through dipolar interactions. Due to fast dynamics of exchange between solution and gel states in the NMR frequency time scale, information was transferred from the hydrogel fibers to the molecules in solution, resulting in strong negative NOEs on the 2D map [26]. Interestingly, several new NOEs appeared in the spectrum of the hydrogel, including cross-peaks between the methyl protons 9 and 11 of Ile and all the aromatic protons of (i) Tyr (H28, H29, H31 and H32) and (ii) H16 of Trp, suggesting a possible folding of the two aromatic regions of Tyr and Trp resulting in a closer proximity to Ile. In addition, protons H9 showed new NOEs with proton H10 β of Ile and the aromatic protons H28 and H29 of Tyr with H26 α , H26 β , and H24 protons of the same residue. Protons H19 and H20 demonstrated weak negative NOEs with proton H14 α,β of Trp, indicating spatial proximity. Additionally, the NOEs between protons H8 and H9 and protons H10 α and H10 β of Ile remained as weak positive NOEs, which was expected since they are attributed to a TOCSY effect and spin-spin diffusion occurs through bonds.

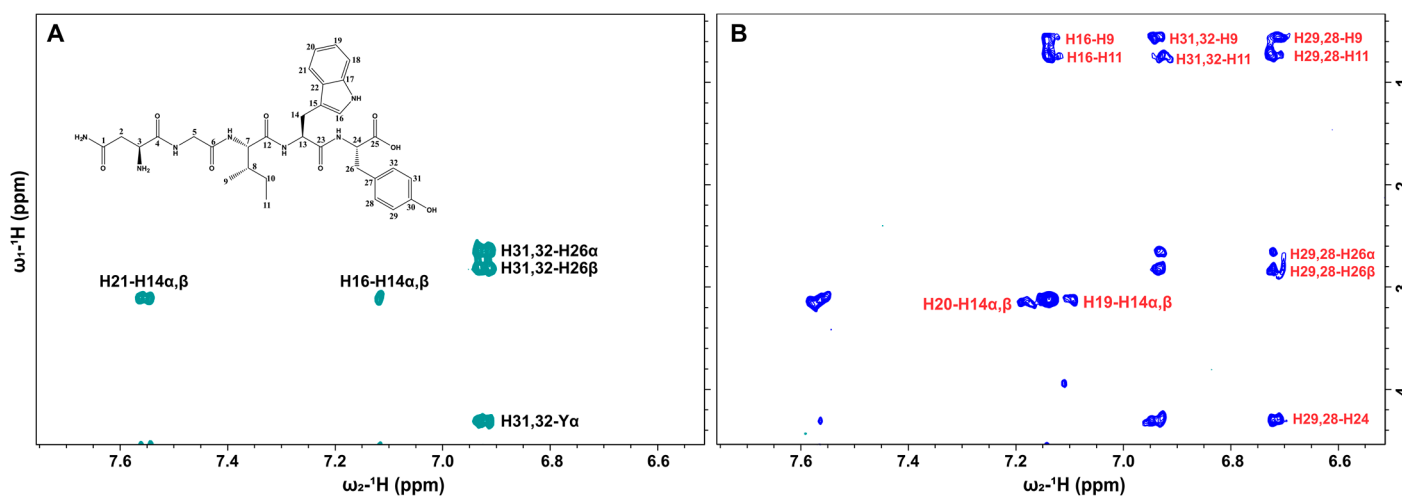


Figure 3. (A) Selective region of 2D NOESY NMR spectrum of NGIWY peptide (1.3 mM) in solution (500 MHz, PBS in D₂O pH 7.4). (B) Selective region of 2D NOESY NMR spectrum of NGIWY peptide (1% *w/v*, 15.3 mM) (500 MHz, PBS in D₂O pH 7.4). New Tr-NOE cross-peaks are denoted with the red color.

3.2.3. Saturation Transfer Difference (STD) NMR

Further investigation of the exchange phenomena between the molecules in the solution state and the molecules incorporated into the hydrogel fiber network was performed with saturation transfer difference (STD) NMR experiments. STD NMR experiments are based on the nuclear Overhauser effect and on the magnetization transfer via spin diffusion from a selectively irradiated macromolecular receptor to the protons of a ligand that are in close contact with the receptor ($\leq 5 \text{ \AA}$) [27]. The applications of STD NMR spectroscopy in the study of supramolecular gels and amino acid-based hydrogels have been investigated very recently [26]. In this case, the hydrogel fibrous network can be considered the macromolecular receptor that is selectively saturated. The selective saturation of the hydrogel can be transferred through the nuclear Overhauser effect throughout the network, resulting in the bound gelator molecules, which are then dissociated back to the pools of water transferring the saturation in the isotropic solution phase. Only the STD signals of the gelator molecules that have been in contact with the hydrogel fibers and have received magnetization transfer will appear in the spectrum. We selectively saturated a region below 0 ppm where only resonances of the network were present and observed STD signals for all the amino acid gelator molecules that received saturation from the fibrous network. The STD signal of Gly H5 was significantly lower compared to the rest of the molecules, possibly indicating a strong binding with longer residence time in the hydrogel network resulting in lower magnetization transfer and less intense STD signals (Figure 4A,B) [25]. We then investigated the magnetization transfer occurring upon the selective irradiation of the H28 and H29 aromatic protons of Tyr residue (Figure 4C–E). In the case of the NGIWY peptide in solution (1.3 mM), except for the nearby H31, H32, H19, H16, and H20 protons, which are within the 0.5 ppm regime of irradiation specificity, no other STD signals appeared in the STD spectrum, suggesting that magnetization was not transferred to the rest of the protons (Figure 4D). On the other hand, when the Tyr aromatic protons H28 and H29 were selectively irradiated in the case of the hydrogel, the STD signals of all the amino acids appeared in the spectrum (Figure 4E). This could be explained by the fact that magnetization was transferred from the gelator molecules to the hydrogel network and from the fibers back to all the protons of the gelators. Again, the STD signal of Gly H5 was lower due to stronger binding.

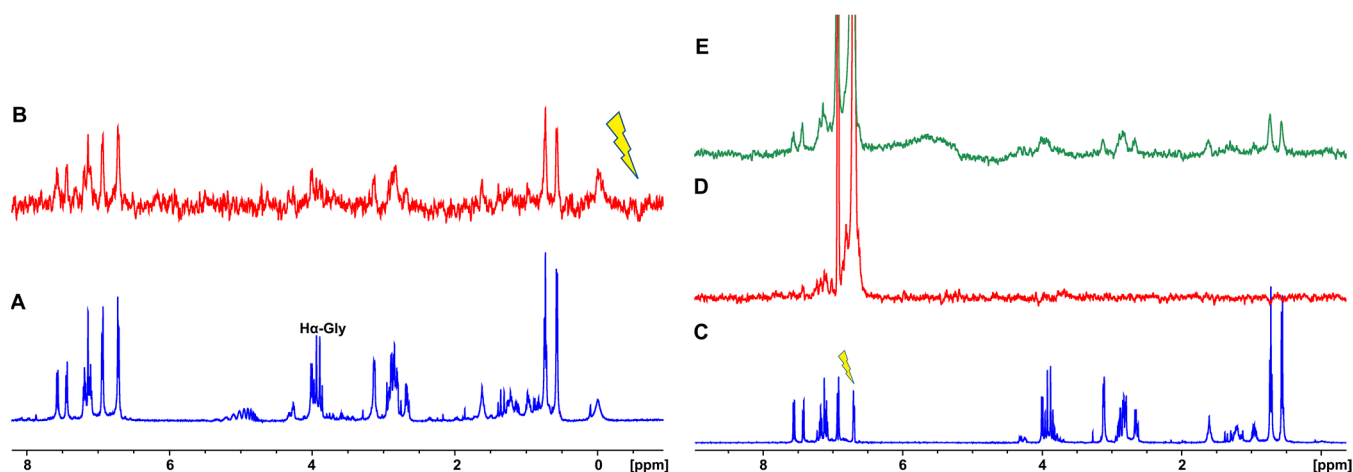


Figure 4. (A) ^1H NMR spectrum of NGIWY (500 MHz, PBS in D_2O pH 7.4). (B) STD NMR spectrum of NGIWY (1% *w/v*, 15.3 mM) peptide (500 MHz, PBS in D_2O pH 7.4). On-resonance selective irradiation occurred at -0.6 ppm. (C) ^1H NMR spectrum of NGIWY (1% *w/v*, 15.3 mM) (500 MHz, PBS in D_2O pH 7.4). (D) STD NMR spectrum of NGIWY peptide (1.3 mM) in solution (500 MHz, PBS in D_2O pH 7.4). On-resonance selective irradiation occurred at 6.70 ppm. (E) STD NMR spectrum of NGIWY (1% *w/v*, 15.3 mM) (500 MHz, PBS in D_2O pH 7.4). On-resonance selective irradiation occurred at 6.70 ppm.

3.3. Molecular Modelling

3.3.1. Molecular Dynamics Simulations

Molecular dynamics (MD) simulations are used to investigate the atomically detailed molecular interactions underlying peptide self-assembly processes. MD simulations provide a reliable method for examining the structural characteristics and conformational dynamics of designed peptides, and they may provide experimentally unavailable insight into the dynamical foundation of self-assembly. We used MD simulations in this study to evaluate the formation of structural characteristics in a peptide system and provide an atomistic view of the nanostructure's self-assembly process. We conducted MD simulations of an empirically confirmed pentapeptide (NGIWY) sequence that may assemble in aqueous conditions to explain the molecular-scale mechanisms related to self-assembly. These extended (200 ns), all-atom simulations were performed in explicit solvent using the AMBER 94 force field. As detailed in several primers, such forcefields represent the physicochemical properties of each amino acid, including partial charges, atomic interaction potentials, and other factors, using a classical, molecular mechanics-based method. In fact, AMBER 94 could be a cutting-edge force field that is applied to a variety of biomolecular systems, particularly peptides [28,29].

The assembly propensity of short peptides correlated with the diffusional association of the NGIWY peptide, according to our models. The peptides took on a variety of aberrant conformations, with transiently stable turns “flickering” into existence. Individuals could be identified in less than 50 ns. NGIWY peptide nanofibers assembled into a β -sheet secondary structure. Extending the simulation further yielded peptides that assembled into two large clusters of tight turns and a random coil by ≈ 200 ns, indicating a structure between the random coil and β -sheet. We used a discrete number-density function to quantify the aggregation propensity of the peptide along its respective trajectories. For NGIWY, a detectable, and presumably hydrophilic-driven, “collapse” of the system appeared to be more kinetically allowed versus other sequences. Visual inspection of trajectories showed a pointy structural reorganization that was timely (<100 ns) in most of the simulations (Figure 5). This random coil formation suggests that the NGIWY peptide is dynamic and that its conformation adapts to its environment. The tight turn depicted in Figure 5 is attributed to the calculated β -turn of the peptide.

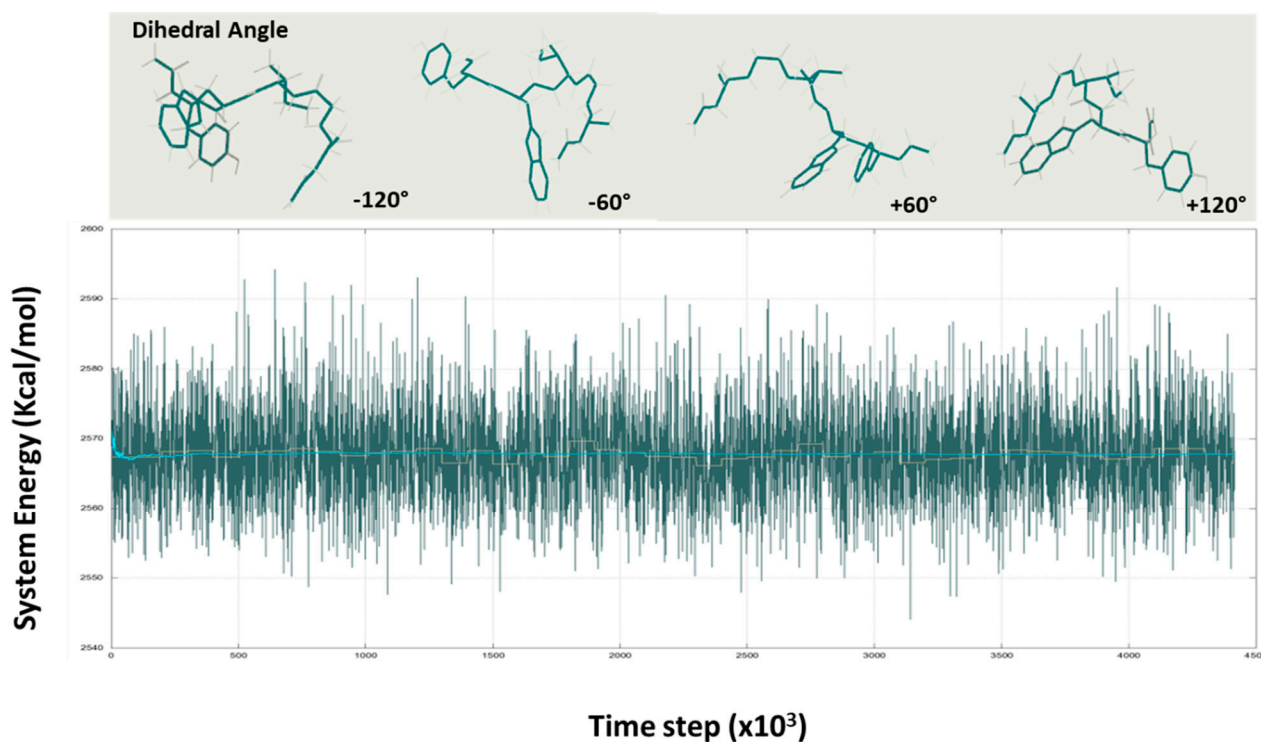


Figure 5. Dihedral angle conformations of the NGIWY peptide and energy formation during the simulation process.

Because the interactions involved in turn formation are mostly local, turns have been argued to be significant in folding because they can commence productive structure creation without a large loss in chain entropy [28]. With the exception of the N- and C-termini, the torsion angles for amino acids suggest significant structural heterogeneity in the system. Our findings imply that the pentapeptide's central Ile frequently adopted a type-II turn conformation ($\varphi = -60^\circ$, $\varphi = 120^\circ$) or an antiparallel sheet structure ($\varphi = -120^\circ$, $\varphi = 60^\circ$), (Figure 4). B-turns are well suited to participating in ligand binding, molecular recognition, protein–protein, or protein–nucleic acid interactions because they are largely surface-exposed, influencing protein activities and intermolecular interactions. Because the interactions involved in turn formation are mostly local, turns have been argued to be significant in folding because they can commence productive structure creation without a large loss in chain entropy [30].

3.3.2. DFT Study

The molecular characteristics of the octanol–water partition coefficient (logP), the Δ_{GAP} energy ($\Delta_{\text{GAP}E}$), and hence the potential of ionization (I), were all indirectly related to biological activity, according to the models. However, the energy of the HOMO orbital (E_{HOMO}), overall absolute charge, and Ghose–Crippen molar refractivity (AMR) are descriptors that were directly associated with the activity and affinity of the peptide. This was likely due to the peptides' electron-rich side-chain residues, which were related to high HOMO properties (Figure 6).

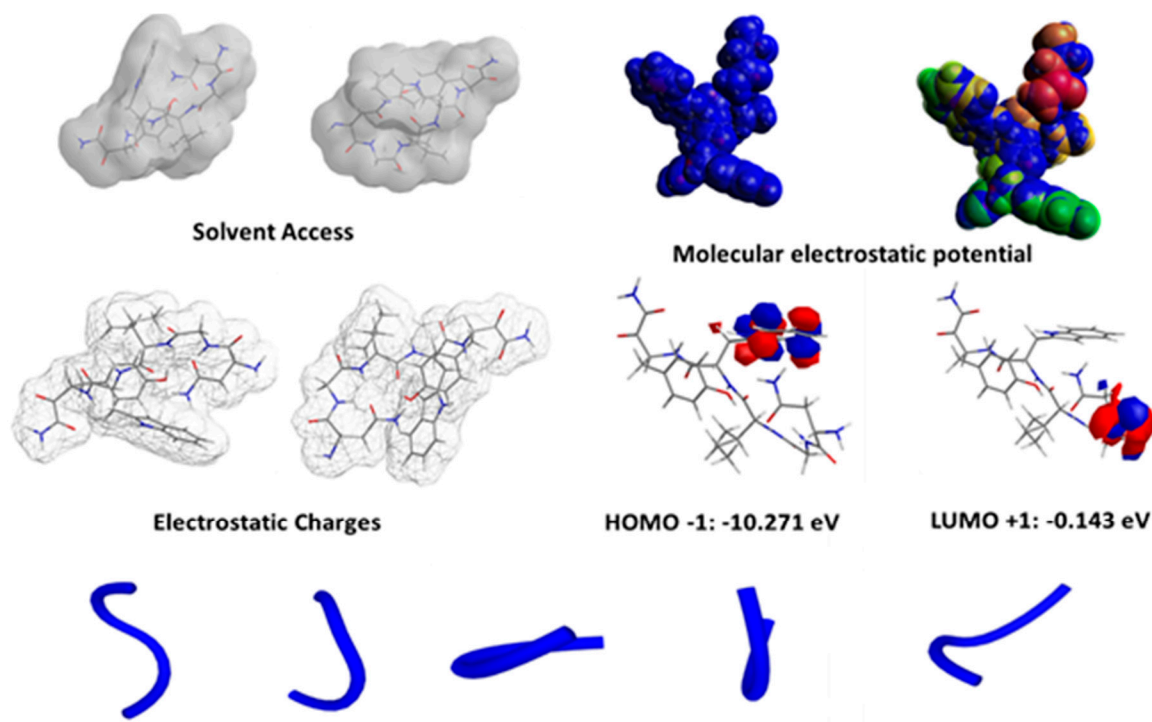


Figure 6. Information received by the DFT studies revealed a fully hydrophilic peptide and an electrostatic potential profile. The MD simulations showed the 5 most possible conformations of the pentapeptide.

ADME models are used to describe biological activity. The thermodynamic and transport properties of the molecular system in Table S2 lists the peptide's molecular properties, and Table S3 shows the values of the topological and molecular descriptors that were used in the simulation algorithm study. The van der Waals attractions between molecules play a role in determining the thermodynamic and transport properties of a chemical system. The electronic polarizability and molar refractivity (AMR) of molecules are linked by van der Waals interactions (or London scattering attractions) (Figure 6). AMR is a constitutive additive feature that can be estimated to account for contributions from within the atom and its connectivity, as well as a variety of correction variables [31,32].

AMR could be a crucial physical–chemical parameter that has contributed significantly to the study of binding electrons in organic compounds in the past. The results of the AMR and charge values show that this ultra-short peptide is comparable to other short peptides from the literature. Furthermore, the descriptors associated with the peptide's water solubility indicate that its activity is linked to its ability to be water soluble, and NGIWY is a very soluble peptide. However, peptides with higher lipophilicity do not present higher biological activity [33].

Quantum mechanical descriptors generated from DFT investigations have been used successfully to justify and explain chemical reactivity in a wide range of applications. One of the most widely used quantum mechanical descriptors is the energy of the highest occupied molecular orbital (EHOMO). The frontier orbitals and their energies are significant in explaining a system's reactivity and are utilized as a marker of high-electron-density locations (Figure 6). As a result, these zones exhibit a positive region to be attacked by electrophile groups.

3.3.3. Binding Free Energy Calculation

The protein–protein docking analysis employed MD simulations to find the most crowded peptide configurations, allowing for the determination of protein sites involved in the recognition process (Figure 5). Docking experiments, on the other hand, do not demonstrate the validity of those interactions in a highly solvated and varied environment.

Because of the initial configurations for the 20 ns-long MD simulation, complexes with the lowest binding free energy generated by docking calculations were frequently chosen. The binding free energy (ΔG_{bind}) without the entropic contribution (ΔTS) was energetically beneficial for the complex, according to this research. However, docking studies do not illustrate the soundness of those interactions in an exceedingly solvated and versatile environment. The electrostatic energy (ΔE_{elec}) and hence the solvation energy (ΔG_{GB}) varied more than the van der Waals dispersion energies (G_{vdw}), as seen in Table S4. The non-polar contributions ($\Delta E_{\text{non-polar}} = \Delta E_{\text{vdw}} + \Delta G_{\text{SA}}$) dominated the net ΔG_{bind} value. The screening effect of the solvent is evident here, with non-polar contributions dominating the total ΔG_{bind} value. These results reveal that the NGIWY peptide experienced the foremost favorable binding free energy with the has receptor, compared to other short peptides from the literature, indicating a great binding result with the transport protein, a promising result for drug delivery systems [34,35]. Structural analysis of the HSA–peptide complex shows that it maintained similar structural conformation together with MD simulations, like those predicted through docking procedures.

3.4. Pentapeptide Hydrogel Preparation and Characterization

3.4.1. Hydrogel Preparation and Rheological Studies

NGIWY-amide pentapeptide was dissolved in Milli-Q water at a 2% (*w/v*) final concentration and sonicated at 25 °C until a clear solution was obtained. The solution was left undisturbed, and a transparent gel was obtained within less than 30 min (Figure S3).

The gelation kinetics and viscoelastic properties of the pentapeptide hydrogel were assessed with rheological analysis. As seen in Figure 7A, the elastic modulus G' was an order of magnitude higher than the loss modulus G'' already from the beginning of the gel-curing experiment, indicating the formation of a firm hydrogel early upon hydration of the pentapeptide. A minor increase in G' at ca. 28 min, observed as change in the slope, denotes the pentapeptide hydrogel's onset of gelation, which continued to stiffen with time (G' max: 160 kPa). Effective gelation depends on the presence of a hydrophobic/hydrophilic balance in the amino acid sequence of a peptide [36,37], in which the presence of aromatic groups has been found to be a facilitator of the gelation process [38]. This observation further supports the experimental findings relative to the pentapeptide sequence containing amino acids (tyrosine and tryptophan) with aromatic moieties. The viscoelastic properties of the pentapeptide hydrogel were monitored immediately after the end of the gel-curing experiments in the frequency range of 0.01–100 rad/s and at 0.1% strain (Figure 7B). The dominance of the elastic response of the pentapeptide hydrogel was evident over the frequency range tested. The storage modulus G' was considerably higher than the loss modulus G'' , indicating the formation of a stiff and stable hydrogel network.

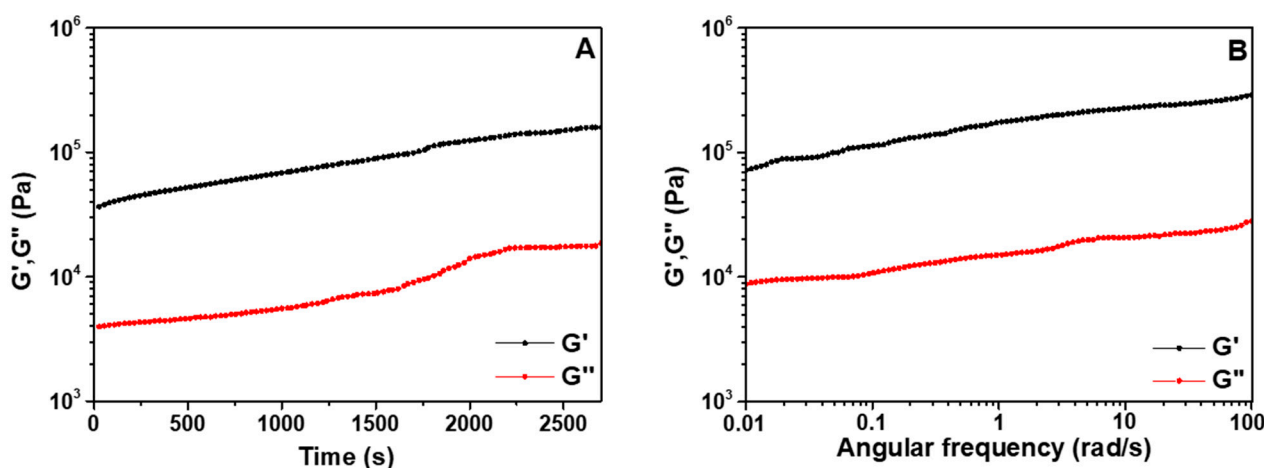


Figure 7. Oscillatory (A) time-sweep and (B) frequency-sweep measurements of the pentapeptide hydrogel (2% *w/v*) at a constant frequency of 1 Hz and strain of 0.1% performed at 25 °C.

3.4.2. Optical Properties, Structural Conformation, and Crystallinity of the Pentapeptide Hydrogel

The light-absorption properties of the pentapeptide hydrogel were investigated by recording its UV-Vis spectrum in aqueous medium (Figure 8A). The most characteristic absorption features of the pentapeptide were observed in the far-UV (<220 nm) and the near-UV regions (280 nm). In particular, the strong absorption peak observed below 220 nm is attributed to the $\pi \rightarrow \pi^*$ transitions of the peptide bonds [39,40] and the carboxylic acid moieties in the peptide [41,42]. The absorption peak at 280 nm is attributed to the aromatic side chains of Trp, with a less intense $\pi \rightarrow \pi^*$ transition identified as a shoulder at 292 nm. Even though less intense, the absorption of Tyr significantly overlapped with that of Trp in the same region. The fluorescence properties of the pentapeptide hydrogel were assessed after dilution of the hydrogel with Milli-Q water at a final concentration of 0.02% *w/v*. The intrinsic fluorescence of the pentapeptide derived from the excitation of Trp and Tyr, with Trp being significantly more fluorescent than Tyr [39]. As seen in Figure 7B, the pentapeptide exhibited a strong emission peak at 354 nm, due to the presence of the indolic ring of Trp. On the other hand, the fluorescence of tyrosine, due to the presence of its phenolic group, was observed as a shoulder at 295 nm [43], since its emission fluorescence was quenched by the presence of the adjacent tryptophan via resonance energy transfer and through ionization of its aromatic hydroxyl group.

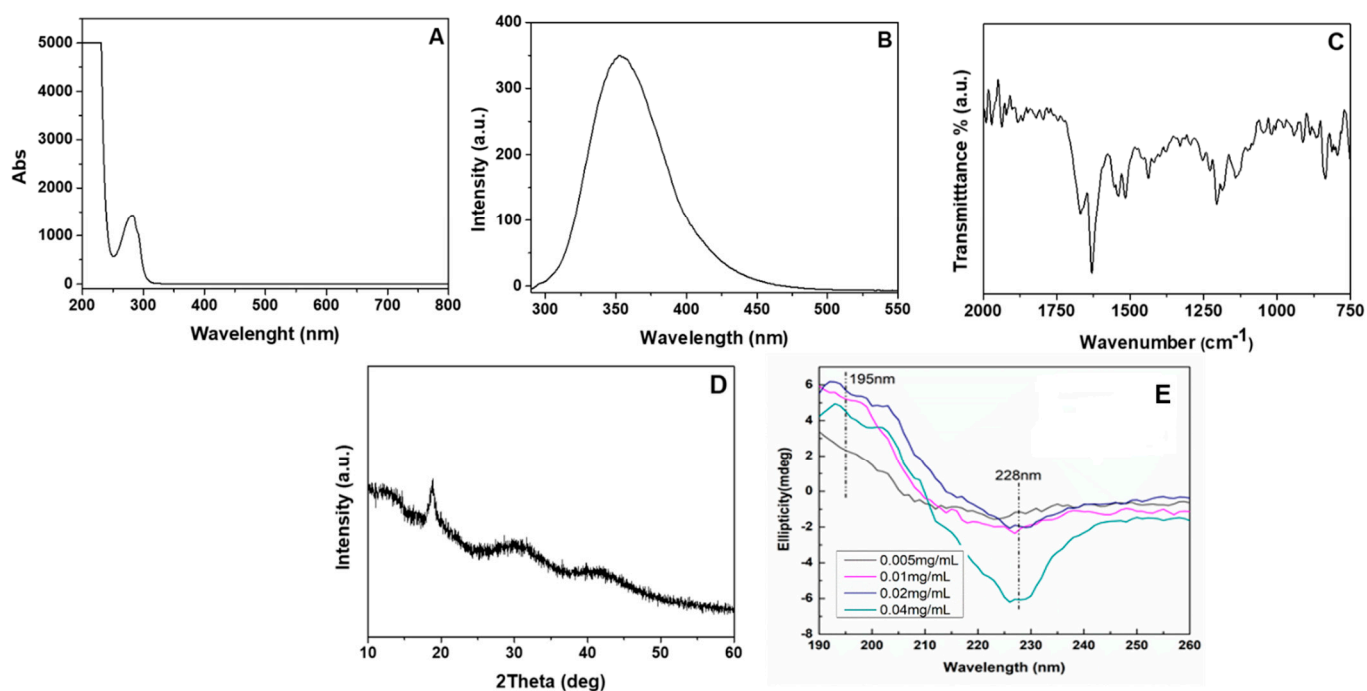


Figure 8. (A) UV adsorption and (B) fluorescence spectra of the pentapeptide hydrogel (0.02% *w/v*) in water. (C) FTIR and (D) XRD diffractogram of the pentapeptide hydrogel. (E) CD spectra of the pentapeptide at different concentrations in double-distilled water at 25 °C.

FT-IR spectroscopy was conducted to evaluate the secondary conformation of the pentapeptide hydrogel (Figure 8C) [44]. The amide I strong absorption band observed at 1629 cm^{-1} is attributed to the stretching vibrations of the C=O and C-N groups [45] and indicates the occurrence of a high β -sheet structure content [46], whereas the peak present at 1668 cm^{-1} suggests the presence of β -turns. Beta sheets that obtain an antiparallel conformation typically demonstrate a weak band at ca. 1690 cm^{-1} [25]. The presence of the high-intensity amide I band at 1629 cm^{-1} and the absence of a weak band at 1690 cm^{-1} suggest the formation of a parallel β -sheet conformation in the pentapeptide hydrogel [27]. Amide II bands observed at 1541 cm^{-1} and 1516 cm^{-1} are associated with N-H bending

vibration and the C-N stretching vibration. XRD analysis was conducted to gain further information on the peptide molecular packing in the hydrogel (Figure 8D). The freeze-dried pentapeptide hydrogel demonstrated a peak at a d-spacing of 4.7 Å ($2\theta = 18.79^\circ$), attributed to the interchain distance expected for β -sheet structures [47]. CD spectroscopy was also employed for the evaluation of the secondary conformation of the pentapeptide at different concentrations (Figure 8E). A positive broad peak around 195–200 nm along with a negative peak at 226–229 nm indicate the presence of a β -sheet like arrangement. The red-shifted β -sheet signal has been previously observed and it has been shown to correlate with a twisted structure [48]. Additionally, the changes observed in the CD spectra as a function of the change in sample concentration are a feature of a self-assembly process that takes place in the solution [49].

3.4.3. Morphological Evaluation of the Pentapeptide Hydrogel

The AFM images of the pentapeptide hydrogel at the concentration of 2% *w/v* demonstrated a surface topology of a network of intertwined nanofibers with helical-twisted morphology (Figure 9A,B dotted rectangles). TEM analysis further verified the findings of AFM studies, showing that the NGIWY-amide pentapeptide was highly filamentous, forming micrometer-long fibers with twisted morphology and a mean diameter of 5.6 ± 1.1 nm. It has been previously shown that a short biomimetic eight amino acid residue peptide derived from squid-sucker ring-teeth proteins gels in water, forming a network of twisted nanofibers with a width of less than 10 nm and a periodicity of 80 nm along the fibers [50]. Experimental findings based on both physicochemical studies and image analysis align well with MD simulations on the possible conformation adopted by the NGIWY-amide pentapeptide, amply indicating for the adoption of a β -turn/ β -sheet secondary structure.

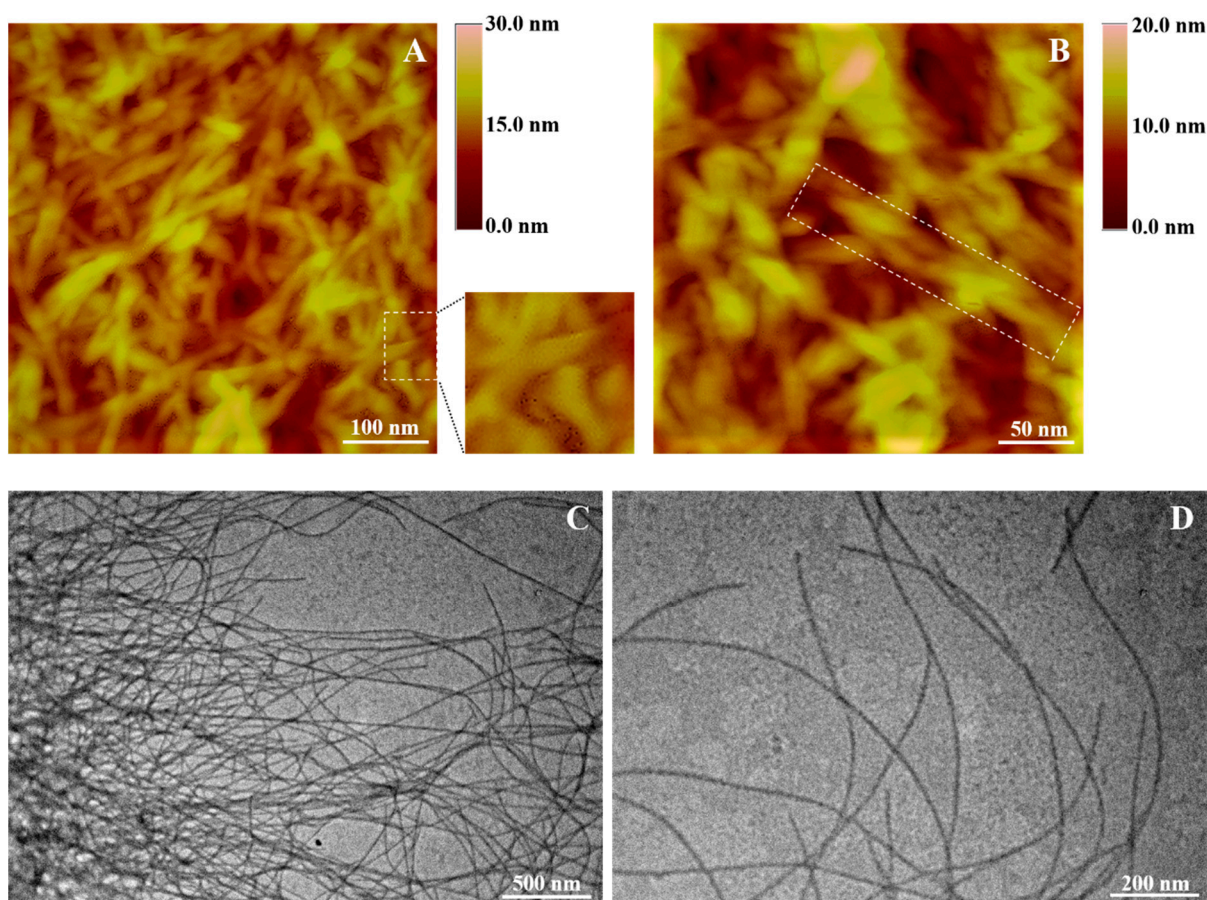


Figure 9. (A,B) AFM images and (C,D) TEM micrographs of the NGIWY-amide pentapeptide hydrogel prepared at 2% *w/v* in Milli-Q water.

3.5. Model Dye Localization in the Hydrogel Network and In Vitro Drug Release Studies

Aiming to identify the suitability of the NGIWY-amide pentapeptide hydrogel as a carrier of both hydrophobic and hydrophilic compounds, the distribution of a lipophilic and a hydrophilic fluorescent dye within the peptide hydrogel was initially evaluated and visualized with CLSM (Figure S4). A strong blue fluorescent signal delineating the peptide nanofiber was evidenced in the presence of Nile blue within the pentapeptide hydrogel, indicating the preferable distribution and interaction of the lipophilic dye with the hydrophobic domains of the pentapeptide. This could translate to a slower dissociation of the lipophilic compound from the nanofibers and a more retarded diffusion towards the aqueous matrix of the hydrogel and further to the surrounding medium. On the contrary, the more hydrophilic calcein demonstrated a more scattered fluorescent signal, suggesting a more preferential distribution within the aqueous environment of the hydrogel rather than within the peptide nanofibers.

In order to verify the CLSM finding, three drugs differing in their molecular weight and aqueous solubility were selected and their in vitro release profiles from the pentapeptide hydrogel (2% *w/v*) were recorded. As shown in Figure 10, octreotide acetate release from the 2% *w/v* hydrogel reached $46.7 \pm 2.4\%$ within the first 2 h, followed by a more sustained release profile for 14 days ($84.1 \pm 3.4\%$). Approximately $66.1 \pm 4.2\%$ doxorubicin release from the 2% *w/v* hydrogel was achieved within the first 4 h, reaching $90.8 \pm 2.0\%$ within 14 days. The slightly slower release rate observed for the macromolecular octreotide acetate compared to the small hydrophilic doxorubicin hydrochloride from the peptide hydrogel, even though not statistically significant ($p > 0.05$), might be attributed to the higher molecular weight of the macromolecule, which delays drug diffusion within the hydrogel pores to the surrounding release medium [7]. Curcumin release from the 2% *w/v* peptide hydrogel reached only $20.2 \pm 2.5\%$ at 48 h, followed by a prolonged release profile for 14 days (81%). The more sustained release observed for curcumin, compared to octreotide acetate and doxorubicin hydrochloride, could be attributed to the drug's hydrophobicity, which, as previously shown [51] and also verified here with the CLSM studies, favors interaction with the peptide nanofiber network, therefore leading to a more retarded release profile. Kinetic analysis of drug release from the pentapeptide hydrogel was performed and the release data of all drugs from the pentapeptide hydrogel correlated best to the Weibull model, as indicated by the respective correlation coefficient values reported in Table S5. The values of the exponent β , which is an indicator of the mechanism of drug transport, were calculated to be less than 0.75, suggesting a Fickian mechanism of drug diffusion through the hydrogel matrix [52]. It was only for curcumin release that β lay within the range of $0.75 < \beta < 1$, indicating a combined mechanism of drug diffusion (Fickian) and swelling-controlled transport [53].

3.6. Cell Viability and Cell Death Assay

In order to detect the cytotoxicity of NGIWY amide, MRC5 and HSC3 cells were allowed to grow in the presence of different concentrations of NGIWY for 24 h, 48 h, and 72 h. The results of cell viability by the Cell Counting Kit-8 (CCK-8) assay revealed that a low concentration of NGIWY (≤ 0.6 mg/mL) had no effect on the viability of MRC5 and HSC3 cells even after 72 h exposure (Figure 11). Additionally, no significant number of dead cells was observed to occur in cultures exposed to the treatments mentioned above as compared to control untreated ones (data not shown). Based on these results of the cell toxicity evaluation, NGIWY amide concentrations at ≤ 0.6 mg/mL were chosen for further experiments.

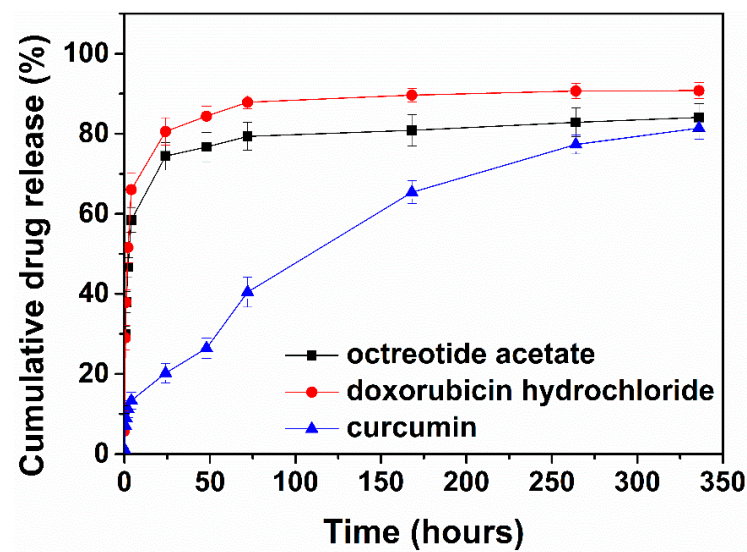


Figure 10. In vitro release profiles of octreotide acetate, doxorubicin hydrochloride, and curcumin from the pentapeptide in PBS pH 7.4 (in the presence of Tween 80 0.1% for curcumin) at 37 °C ($n = 3$, \pm S.D.).

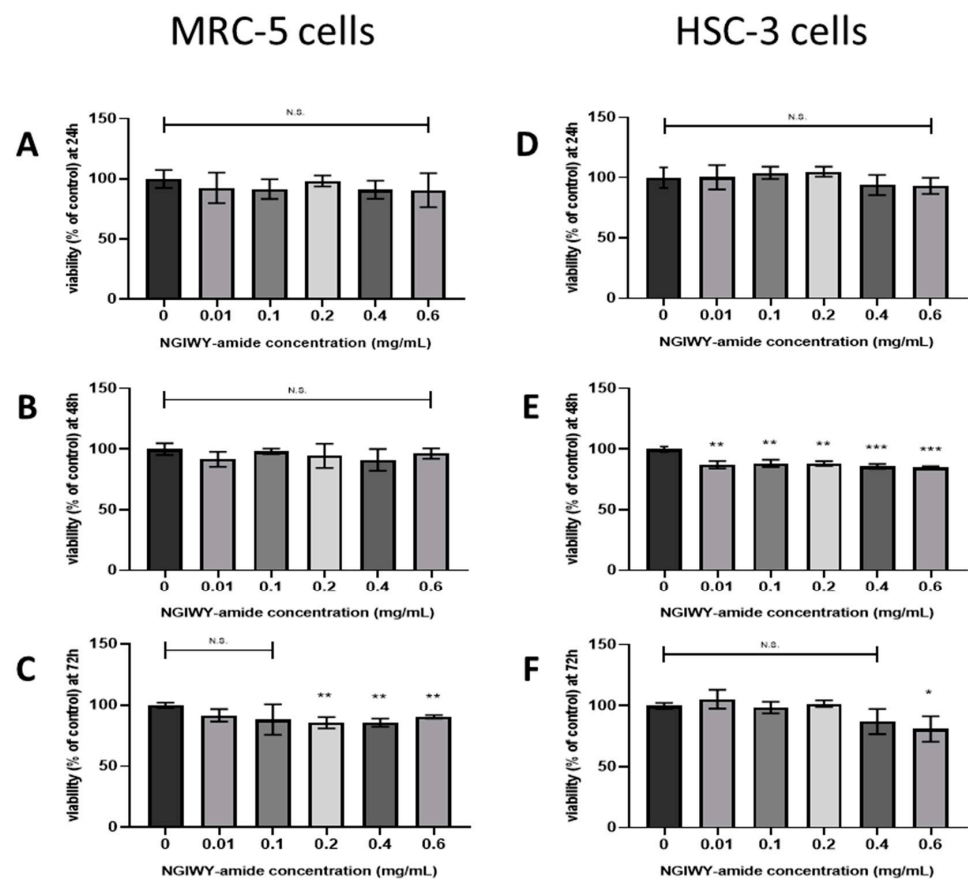


Figure 11. Cytotoxicity evaluation of the NGIWY-amide hydrogel. (A–C) Effect of NGIWY on MRC5 cell survival as assessed by CCK-8 analysis after treating with various concentrations of the NGIWY-amide pentapeptide hydrogel for (A) 24 h, (B) 48 h, and (C) 72 h. (D–F) Effect of NGIWY on HSC3 cells survival as assessed by CCK-8 analysis after treating with various dosages of NGIWY for (D) 24 h, (E) 48 h, and (F) 72 h. The data were analyzed using a *t*-test. Statistical significance was set at $p < 0.05$ (*: $p < 0.05$; **: $p < 0.005$; ***: $p < 0.001$).

4. Discussion

In this study, we outlined and expanded on the properties of an ultra-short self-assembled cosmetic pentapeptide isolated from a marine invertebrate *Apostichopus japonicus* NGIWY-amide. Another cosmetic peptide, palmitoyl-KTTKS, has already been developed and commercialized as peptide hydrogel by Sederma Inc (France) under the brand name Matrixyl™.

NGIWY-amide is a short marine pentapeptide with straightforward production with low-cost peptide synthesis incorporating Trp, an amino acid known for its intrinsic fluorescence. This inherent property enables the recording of its distribution and metabolism inside living cells without additional conjugation with fluorescent dye for labeling. However, aromatic stacking during assembly quenches tryptophan fluorescence [54]. Moreover, the pentapeptide displays excellent solubility in water, making it a promising candidate for several biocompatible applications. Tyrosine at the C-terminal site of the peptide enables the design and synthesis of phosphorylated analogs to form hydrogels in situ after their dephosphorylation in the presence of alkaline phosphatase, a common methodology in short-peptide hydrogels carrying Tyr [55–57]. NMR studies (Figures 2–4) and MD simulations (Figures 5 and 6) as well as spectroscopy and microscopy techniques were used to explore the robust pentapeptide hydrogel's physicochemical parameters and structural properties (morphology, dimensions, etc.), identifying its potential as drug delivery system encapsulating curcumin, doxorubicin, and octreotide; drug molecules with different molecular weight; and aqueous solubility. Through π - π stacking interactions, various collagen like peptides assemble into higher hierarchical-ordered structures and mimic the fibril formation [58]. Li et al. reported that aromatic–aromatic interactions promote the pentapeptide transform from α -helix to β -sheet conformation, although isolated short peptides usually are unable to maintain their original secondary structures [59]. Self-assembled β -sheet peptides tend to form long fibrillar structures or tapes. TEM analysis further verified the findings of AFM studies, showing that the NGIWY-amide pentapeptide was highly filamentous, forming micrometer-long fibers with twisted morphology and a mean diameter of 5.6 ± 1.1 nm (Figure 9). Similar results were presented by Krysmann et al. for the KVLFF, an amyloid peptide fragment that forms fibrils itself in PBS (pH 7.4) [54]. In the same study, the long, stiff fibrils of the peptide hydrogel KLVFF exhibited a mean diameter of 9.68 ± 0.92 nm, and gelation took approximately 15 h for a 2.5% *w/v* sample, decreasing to 2 h for samples with concentrations of 3.0–4.0 *w/v*. However, NGIWY-amide needs less than 30 min to gel even at 1% *w/v*. It has been very recently shown that a short biomimetic eight amino acid residue peptide derived from squid-sucker ring-teeth proteins gels in water, forming a network of twisted nanofibers with a width of less than 10 nm and a periodicity of 80 nm along the fibers [50]. Tang et al. previously published [45] a class of rapidly assembling pentapeptides (KYFIL and analogs) for injectable delivery (RAPID) that form hydrogels with nanofiber structures. They also suggested that the deprotonated C-terminal site is necessary for the gelation of the peptide. This robust peptide hydrogel family is formed spontaneously at a low weight percentage (1.5 to 3% *w/v*), exhibiting a broad range of mechanical properties (50–17,000 Pa) that can be fine-tuned via small changes in concentration or pH. In addition, their rheological experiments indicated that Ile facilitates self-assembly. Further, NGIWY-amide, which incorporates the two aromatic amino acids at the C-terminal site, exhibited stiffness with a storage moduli G' (G' max:160 kPa) (Figure 7). In peptide self-assembly, aromatic (Phe, Trp, Tyr) and aliphatic amino acids (Ala, Ile, Leu, Val) aggregate through π - π stacking and hydrophobic interactions, whereas the polar amino acids stabilize through electrostatic interactions or hydrogen bonds, depending on the charged residues. Predicting the molecular forces after peptide self-assembly is rather difficult without extra facts about the interactions of these forces.

One of the major drawbacks to the development of hydrogels as drug delivery systems is their inability to efficiently entrap and release poorly water-soluble drugs due to their own hydrophilic structure, and if it occurs, a burst release results in toxicity at the site of administration. Thus, NGIWY-amide delivered antitumor drugs of various molecular

weight and hydrophobicity. The water-insoluble curcumin demonstrated a prolonged release profile for 14 days, in comparison to doxorubicin and octreotide acetate. Entrapment of the water-insoluble curcumin displayed a uniform distribution inside the gel with no observable aggregates. The high-MW (~1000) peptide octreotide acetate displayed a slightly slower release rate compared to the small molecule doxorubicin hydrochloride (~500), which might be attributed to the higher molecular weight of the macromolecule, which delays drug diffusion within the hydrogel pores to the surrounding release medium. The hydrochloric and acetate salts in doxorubicin and octreotide, respectively, disrupted the ionic interaction of the peptide hydrogel and enhanced the high release rate. On the opposite side, the lipophilic curcumin exhibited a more sustained release and favored the interaction with the peptide nanofiber network, therefore leading to a more retarded release. Short to ultra-short peptide hydrogels have already been used to deliver antitumor drugs such as doxorubicin [60–62] and curcumin [63–65]. In most cases, the synthesized peptides are based on the homodipeptide FF or its modified natural or unnatural amino acids, like naphthylalanine. Gelation kinetics and the drug release over time are dependent on the peptide sequence. Recently, doxorubicin entrapped in a short nucleo-peptide hydrogel (Ade-FFF) released at a sustained rate (55% over 12 days) [66]. Other researchers used doxil instead of doxorubicin hydrochloride, so their results are not comparable, as doxil (the liposomal formula of doxorubicin) is expected to exhibit a different release rate [61]. Four different α,β -dehydrophenylalanine dipeptide nanotubes were used to encapsulate curcumin and investigate the management of malaria [64]. Eighty percent of the initial loaded curcumin concentration needed almost 90 h to be released from the nanosystem. Zhuo et al. reported a short rationally designed peptide hydrogel incorporating the Fmoc group an ocular implant for the prolonged release of antiproliferative drug 5-fluorouracil (5-FU); after 7 days, almost the total loaded 5-FU was released from the hydrogel [66].

Finally, the NGIWY-amide peptide hydrogel, a new candidate material for local drug delivery or other biomedical applications, was tested for its biocompatibility, a prerequisite criterion for clinical use. Biocompatibility of the pentapeptide hydrogel was assessed by CCK-8 analysis after treating both normal MRC5 and cancer HSC3 cells with various concentrations of the NGIWY-amide pentapeptide hydrogel (Figure 11). The results indicate that the growth of cells was unaffected, as no cytotoxicity was observed and the gel exhibited high biocompatibility.

5. Conclusions

In summary, we demonstrated for the first time the self-assembling properties of a natural known marine peptide (NGIWY-amide) isolated from sea cucumber *Apostichopus japonicus* and explored the robust hydrogel's physicochemical parameters and its potential as a drug delivery system. NMR studies and MD simulations as well as spectroscopy and microscopy techniques were used to explore and identify the structural properties of the self-assembling peptide. Overall, the peptide hydrogel demonstrated (i) straightforward low-cost synthesis, (ii) gelation simplicity under physiological conditions, (iii) formation of a firm hydrogel, (iv) a simple encapsulation procedure, and (v) release of both hydrophobic and hydrophilic drug molecules and macromolecules in a controlled manner. NGIWY-amide peptide hydrogel addresses many of the drawbacks associated with existing peptide hydrogels for delivering therapeutics and is thus a promising candidate for further investigation as an in-situ gel-forming depot system for encapsulation and controlled drug delivery. Additionally, we observed hierarchical nanostructures (individuals nanofibers) that may offer new approaches for cell growth, drug delivery, regenerative medicine, tissue engineering, and 3D-printing-based tissue manufacturing even though bioelectronics. The field of bioinspired ultra-short self-assembling peptides is comparably new; novel discoveries and materials are expected to be explored and exploited for several future research directions and applications. We firmly believe that peptides from marine organisms like invertebrates and echinoderms pave new horizons in biomedicine.

Supplementary Materials: The following supporting information can be downloaded at: <https://www.mdpi.com/article/10.3390/pharmaceutics14010133/s1>, Table S1: ^1H and ^{13}C NMR chemical shifts of NGIWY in D_2O , Table S2: ADME molecular properties of the pentapeptide, Table S3: MM2 job type, Table S4: Binding energy distribution of the NGIWY-amide with the transport protein, Table S5: Release kinetic parameters of octreotide acetate, doxorubicin hydrochloride, and curcumin from the pentapeptide hydrogel, Figure S1: Structure of the NGIWY-amide, Figure S2: HPLC profile of the synthesized peptide at 220 nm, Figure S3: Mass spectrum of the main peak at 10.79 min (PDF), Figure S4: Inverted vial of the hydrogel of the peptide.

Author Contributions: N.F.T., methodology, investigation, data curation, writing—original draft preparation, writing—review and editing; C.K., methodology, investigation, data curation, writing—original draft preparation, writing—review and editing; M.C.V., software, formal analysis, writing—original draft preparation; A.P., methodology, investigation, data curation, writing—original draft preparation; C.N., investigation; A.V.C., investigation, data curation; A.-T.C., investigation, data curation, writing—original draft preparation; C.P., data curation, resources, writing—review and editing; N.B., data curation, resources, writing—review and editing; C.K.Z., methodology, investigation, data curation, writing—review and editing; E.G., data curation, resources, writing—review and editing; Y.S., conceptualization, methodology, investigation, data curation, writing—original draft preparation, writing—review and editing; D.G.F., conceptualization, resources, writing—review and editing; I.S.V., conceptualization, resources, writing—review and editing, supervision, project administration. All authors have read and agreed to the published version of the manuscript.

Funding: This study was supported by the interdepartmental funds of Aristotle University of Thessaloniki, Greece, and the University of Nicosia, Cyprus. This research was co-financed by Greece and the European Union (European Social Fund-ESF) through the Operational Program “Human Resources Development, Education and Lifelong Learning” in the context of the project “Strengthening Human Resources Research Potential via Doctorate Research—2nd cycle” (MIS 5000432, implemented by the State Scholarships Foundation (IKY) awarded to N.F.T.

Data Availability Statement: The raw/processed data required to reproduce these findings cannot be shared at this time, as the data also forms part of an ongoing study.

Acknowledgments: We would like to acknowledge the Network of Research Supporting Laboratories at the University of Ioannina for using the Nuclear Magnetic Resonance Spectroscopy Center and the Biotechnology Laboratory of the University of Ioannina for providing access to the circular dichroism facilities. The authors gratefully acknowledge Evangelos Karoutsos for the AFM images and Mary Kollia and the Laboratory of Electron Microscopy and Microanalysis, School of Natural Sciences, University of Patras, for the TEM measurements.

Conflicts of Interest: The authors declare no conflict of interest. The funders had no role in the design of the study; in the collection, analyses, or interpretation of data; in the writing of the manuscript, or in the decision to publish the results.

References

1. Hamley, I.W. Small Bioactive Peptides for Biomaterials Design and Therapeutics. *Chem. Rev.* **2017**, *117*, 14015–14041. [[CrossRef](#)] [[PubMed](#)]
2. Kurbasic, M.; Parisi, E.; Garcia, A.M.; Marchesan, S. Self-Assembling, Ultrashort Peptide Gels as Antimicrobial Biomaterials. *Curr. Top. Med. Chem.* **2020**, *20*, 1300–1309. [[CrossRef](#)] [[PubMed](#)]
3. Ni, M.; Zhuo, S. Applications of self-assembling ultrashort peptides in bionanotechnology. *RSC Adv.* **2019**, *9*, 844–852. [[CrossRef](#)]
4. Garcia, A.M.; Melchionna, M.; Bellotto, O.; Kralj, S.; Semeraro, S.; Parisi, E.; Iglesias, D.; D’Andrea, P.; De Zorzi, R.; Vargiu, A.V.; et al. Nanoscale Assembly of Functional Peptides with Divergent Programming Elements. *ACS Nano* **2021**, *15*, 3015–3025. [[CrossRef](#)]
5. Malonis, R.J.; Lai, J.R.; Vergnolle, O. Peptide-Based Vaccines: Current Progress and Future Challenges. *Chem. Rev.* **2019**, *120*, 3210–3229. [[CrossRef](#)]
6. Tesauro, D.; Accardo, A.; Diaferia, C.; Milano, V.; Guillon, J.; Ronga, L.; Rossi, F. Peptide-Based Drug-Delivery Systems in Biotechnological Applications: Recent Advances and Perspectives. *Molecules* **2019**, *24*, 351. [[CrossRef](#)]
7. Li, Y.; Wang, F.; Cui, H. Peptide-based supramolecular hydrogels for delivery of biologics. *Bioeng. Transl. Med.* **2016**, *1*, 306–322. [[CrossRef](#)]
8. Gupta, S.; Singh, I.; Sharma, A.K.; Kumar, P. Ultrashort Peptide Self-Assembly: Front-Runners to Transport Drug and Gene Cargos. *Front. Bioeng. Biotechnol.* **2020**, *8*, 504. [[CrossRef](#)]

9. Errante, F.; Ledwoń, P.; Latajka, R.; Rovero, P.; Papini, A.M. Cosmeceutical Peptides in the Framework of Sustainable Wellness Economy. *Front. Chem.* **2020**, *8*, 572923. [[CrossRef](#)] [[PubMed](#)]
10. Das, R.; Gayakvad, B.; Shinde, S.D.; Rani, J.; Jain, A.; Sahu, B. Ultrashort Peptides—A Glimpse into the Structural Modifications and Their Applications as Biomaterials. *ACS Appl. Biol. Mater.* **2020**, *3*, 5474–5499. [[CrossRef](#)]
11. Okesola, B.O.; Wu, Y.; Derkus, B.; Gani, S.; Wu, D.; Knani, D.; Smith, D.K.; Adams, D.J.; Mata, A. Supramolecular Self-Assembly To Control Structural and Biological Properties of Multicomponent Hydrogels. *Chem. Mater.* **2019**, *31*, 7883–7897. [[CrossRef](#)]
12. Schnaider, L.; Shimonov, L.; Kreiser, T.; Zaguri, D.; Bychenko, D.; Brickner, I.; Kolusheva, S.; Lichtenstein, A.; Kost, J.; Gazit, E. Ultrashort Cell-Penetrating Peptides for Enhanced Sonophoresis-Mediated Transdermal Transport. *ACS Appl. Biol. Mater.* **2020**, *3*, 8395–8401. [[CrossRef](#)]
13. Susapto, H.H.; Alhattab, D.; Abdelrahman, S.; Khan, Z.; Alshehri, S.; Kahin, K.; Ge, R.; Moretti, M.; Emwas, A.-H.; Hauser, C.A.E. Ultrashort Peptide Bioinks Support Automated Printing of Large-Scale Constructs Assuring Long-Term Survival of Printed Tissue Constructs. *Nano Lett.* **2021**, *21*, 2719–2729. [[CrossRef](#)] [[PubMed](#)]
14. Rauf, S.; Susapto, H.H.; Kahin, K.; Alshehri, S.; Abdelrahman, S.; Lam, J.H.; Asad, S.; Jadhav, S.; Sundaramurthi, D.; Gao, X.; et al. Self-assembling tetrameric peptides allow in situ 3D bioprinting under physiological conditions. *J. Mater. Chem. B* **2021**, *9*, 1069–1081. [[CrossRef](#)] [[PubMed](#)]
15. MacPherson, D.; Bram, Y.; Park, J.; Schwartz, R.E. Peptide-based scaffolds for the culture and maintenance of primary human hepatocytes. *Sci. Rep.* **2021**, *11*, 6772. [[CrossRef](#)]
16. Seow, W.Y.; Hauser, C.A.E. Short to ultrashort peptide hydrogels for biomedical uses. *Mater. Today* **2014**, *17*, 381–388. [[CrossRef](#)]
17. Peressotti, S.; Koehl, G.E.; Goding, J.A.; Green, R.A. Self-Assembling Hydrogel Structures for Neural Tissue Repair. *ACS Biomater. Sci. Eng.* **2021**, *7*, 4136–4163. [[CrossRef](#)] [[PubMed](#)]
18. Wei, G.; Su, Z.; Reynolds, N.P.; Arosio, P.; Hamley, I.W.; Gazit, E.; Mezzenga, R. Self-assembling peptide and protein amyloids: From structure to tailored function in nanotechnology. *Chem. Soc. Rev.* **2017**, *46*, 4661–4708. [[CrossRef](#)]
19. Levin, A.; Hakala, T.A.; Schnaider, L.; Bernardes, G.J.L.; Gazit, E.; Knowles, T.P.J. Biomimetic peptide self-assembly for functional materials. *Nat. Rev. Chem.* **2020**, *4*, 615–634. [[CrossRef](#)]
20. Inoue, M.; Birenheide, R.; Koizumi, O.; Kobayakawa, Y.; Muneoka, Y.; Motokawa, T. Localization of the neuropeptide NGI-WYamide in the holothurian nervous system and its effects on muscular contraction. *Proc. R. Soc. Lond. Ser. B Biol. Sci.* **1999**, *266*, 993–1000. [[CrossRef](#)]
21. Kato, S.; Tsurumaru, S.; Taga, M.; Yamane, T.; Shibata, Y.; Ohno, K.; Fujiwara, A.; Yamano, K.; Yoshikuni, M. Neuronal peptides induce oocyte maturation and gamete spawning of sea cucumber, *Apostichopus japonicus*. *Dev. Biol.* **2009**, *326*, 169–176. [[CrossRef](#)] [[PubMed](#)]
22. Siahaan, E.A.; Pangestuti, R.; Munandar, H.; Kim, S.K. Cosmeceuticals properties of sea cucumbers: Prospects and trends. *Cosmetics* **2017**, *4*, 26. [[CrossRef](#)]
23. Chakraborty, P.; Gazit, E. Amino Acid Based Self-assembled Nanostructures: Complex Structures from Remarkably Simple Building Blocks. *ChemNanoMat* **2018**, *4*, 730–740. [[CrossRef](#)] [[PubMed](#)]
24. Vizirianakis, I.S.; Tsiftoglou, A.S. Blockade of murine erythroleukemia cell differentiation by hypomethylating agents causes accumulation of discrete small poly(A)- RNAs hybridized to 3'-end flanking sequences of β major globin gene. *Biochim. Biophys. Acta-Mol. Cell Res.* **2005**, *1743*, 101–114. [[CrossRef](#)]
25. Yamada, N.; Ariga, K.; Naito, M.; Matsubara, K.; Koyama, E. Regulation of beta-sheet structures within amyloid-like beta-sheet assemblage from tripeptide derivatives. *J. Am. Chem. Soc.* **1998**, *120*, 12192–12199. [[CrossRef](#)]
26. Ramalhete, S.M.; Nartowski, K.P.; Sarathchandra, N.; Foster, J.S.; Round, A.N.; Angulo, J.; Lloyd, G.O.; Khimyak, Y.Z. Supramolecular Amino Acid Based Hydrogels: Probing the Contribution of Additive Molecules using NMR Spectroscopy. *Chem.-A Eur. J.* **2017**, *23*, 8014–8024. [[CrossRef](#)]
27. Ganesh, S.; Prakash, S.; Jayakumar, R. Spectroscopic investigation on gel-forming β -sheet assemblage of peptide derivatives. *Biopolymers* **2003**, *70*, 346–354. [[CrossRef](#)] [[PubMed](#)]
28. Bartels, C.; Widmer, A.; Ehrhardt, C. Absolute free energies of binding of peptide Analogs to the HIV-1 protease from molecular dynamics simulations. *J. Comput. Chem.* **2005**, *26*, 1294–1305. [[CrossRef](#)]
29. Marcelino, A.M.C.; Gierasch, L.M. Roles of β -turns in protein folding: From peptide models to protein engineering. *Biopolymers* **2008**, *89*, 380–391. [[CrossRef](#)]
30. Xiong, H.; Buckwalter, B.L.; Shieh, H.M.; Hecht, M.H. Periodicity of polar and nonpolar amino acids is the major determinant of secondary structure in self-assembling oligomeric peptides. *Proc. Natl. Acad. Sci. USA* **1995**, *92*, 6349–6353. [[CrossRef](#)]
31. Chowdhury, S.M.; Talukder, S.A.; Khan, A.M.; Afrin, N.; Ali, M.A.; Islam, R.; Parves, R.; Al Mamun, A.; Sufian, M.A.; Hossain, M.N.; et al. Antiviral Peptides as Promising Therapeutics against SARS-CoV-2. *J. Phys. Chem. B* **2020**, *124*, 9785–9792. [[CrossRef](#)]
32. Andrade-Ochoa, S.; García-Machorro, J.; Bello, M.; Rodríguez-Valdez, L.M.; Flores-Sandoval, C.A.; Correa-Basurto, J. QSAR, DFT and molecular modeling studies of peptides from HIV-1 to describe their recognition properties by MHC-I. *J. Biomol. Struct. Dyn.* **2018**, *36*, 2312–2330. [[CrossRef](#)]
33. Horne, D.S. Casein structure, self-assembly and gelation. *Curr. Opin. Colloid Interface Sci.* **2002**, *7*, 456–461. [[CrossRef](#)]

34. Aghaee, E.; Ghasemi, J.B.; Manouchehri, F.; Balalaie, S. Combined docking, molecular dynamics simulations and spectroscopic studies for the rational design of a dipeptide ligand for affinity chromatography separation of human serum albumin. *J. Mol. Model.* **2014**, *20*, 2446. [[CrossRef](#)] [[PubMed](#)]
35. Sivertsen, A.; Isaksson, J.; Leiros, H.K.S.; Svenson, J.; Svendsen, J.S.; Brandsdal, B.O. Synthetic cationic antimicrobial peptides bind with their hydrophobic parts to drug site II of human serum albumin. *BMC Struct. Biol.* **2014**, *14*, 4. [[CrossRef](#)]
36. Maity, I.; Manna, M.K.; Rasale, D.B.; Das, A.K. Peptide-Nanofiber-Supported Palladium Nanoparticles as an Efficient Catalyst for the Removal of N-Terminus Protecting Groups. *Chempluschem* **2014**, *79*, 413–420. [[CrossRef](#)] [[PubMed](#)]
37. Yan, C.; Pochan, D.J. Rheological properties of peptide-based hydrogels for biomedical and other applications. *Chem. Soc. Rev.* **2010**, *39*, 3528–3540. [[CrossRef](#)]
38. Fleming, S.; Ulijn, R.V. Design of nanostructures based on aromatic peptide amphiphiles. *Chem. Soc. Rev.* **2014**, *43*, 8150–8177. [[CrossRef](#)]
39. Antosiewicz, J.M.; Shugar, D. UV-Vis spectroscopy of tyrosine side-groups in studies of protein structure. Part 2: Selected applications. *Biophys. Rev.* **2016**, *8*, 163–177. [[CrossRef](#)]
40. Sharma, B.; Asher, S.A. UV resonance Raman finds peptide bond-Arg side chain electronic interactions. *J. Phys. Chem. B* **2011**, *115*, 5659–5664. [[CrossRef](#)]
41. Mcconnell, J.S.; Mcconnell, R.M.; Hossner, L.R. Ultraviolet Spectra of Acetic Acid, Glycine, and Glyphosate. *J. Ark. Acad. Sci.* **1993**, *47*, 73–76.
42. Willard, M.; Cowan, W.M.; Vagelos, P.R. The polypeptide composition of intra-axonally transported proteins: Evidence for four transport velocities. *Proc. Natl. Acad. Sci. USA* **1974**, *71*, 2183–2187. [[CrossRef](#)]
43. Edelhoch, H.; Lippoldt, R.E. Structural studies on polypeptide hormones. I. Fluorescence. *J. Biol. Chem.* **1969**, *244*, 3876–3883. [[CrossRef](#)]
44. Barth, A. Infrared spectroscopy of proteins. *Biochim. Biophys. Acta-Bioenerg.* **2007**, *1767*, 1073–1101. [[CrossRef](#)]
45. Tang, J.D.; Mura, C.; Lampe, K.J. Stimuli-Responsive, Pentapeptide, Nanofiber Hydrogel for Tissue Engineering. *J. Am. Chem. Soc.* **2019**, *141*, 4886–4899. [[CrossRef](#)] [[PubMed](#)]
46. Pazderková, M.; Maloň, P.; Zíma, V.; Hofbauerová, K.; Kopecký, V., Jr.; Kočíšová, E.; Pazderka, T.; Čerovský, V.; Bednářová, L. Interaction of Halictine-Related Antimicrobial Peptides with Membrane Models. *Int. J. Mol. Sci.* **2019**, *20*, 631. [[CrossRef](#)]
47. Sharma, P.; Kaur, H.; Roy, S. Designing a Tenascin-C-Inspired Short Bioactive Peptide Scaffold to Direct and Control Cellular Behavior. *ACS Biomater. Sci. Eng.* **2019**, *5*, 6497–6510. [[CrossRef](#)] [[PubMed](#)]
48. Kaur, H.; Sharma, P.; Patel, N.; Pal, V.K.; Roy, S. Accessing Highly Tunable Nanostructured Hydrogels in a Short Ionic Complementary Peptide Sequence via pH Trigger. *Langmuir* **2020**, *36*, 12107–12120. [[CrossRef](#)]
49. Pignataro, M.F.; Herrera, M.G.; Doderio, V.I. Evaluation of Peptide/Protein Self-Assembly and Aggregation by Spectroscopic Methods. *Molecules* **2020**, *25*, 4854. [[CrossRef](#)]
50. Hiew, S.H.; Mohanram, H.; Ning, L.; Guo, J.; Sánchez-Ferrer, A.; Shi, X.; Pervushin, K.; Mu, Y.; Mezzenga, R.; Miserez, A. A Short Peptide Hydrogel with High Stiffness Induced by 310-Helices to β -Sheet Transition in Water. *Adv. Sci.* **2019**, *6*, 1901173. [[CrossRef](#)] [[PubMed](#)]
51. Karavasilis, C.; Panteris, E.; Vizirianakis, I.S.; Koutsopoulos, S.; Fatouros, D.G. Chemotherapeutic Delivery from a Self-Assembling Peptide Nanofiber Hydrogel for the Management of Glioblastoma. *Pharm. Res.* **2018**, *35*, 166. [[CrossRef](#)] [[PubMed](#)]
52. Papadopoulou, V.; Kosmidis, K.; Vlachou, M.; Macheras, P. On the use of the Weibull function for the discernment of drug release mechanisms. *Int. J. Pharm.* **2006**, *309*, 44–50. [[CrossRef](#)] [[PubMed](#)]
53. Kosmidis, K.; Argyrakos, P.; Macheras, P. A Reappraisal of Drug Release Laws Using Monte Carlo Simulations: The Prevalence of the Weibull Function. *Pharm. Res.* **2003**, *20*, 988–995. [[CrossRef](#)] [[PubMed](#)]
54. Krysmann, M.J.; Castelletto, V.; Kelarakis, A.; Hamley, I.W.; Hule, R.A.; Pochan, D.J. Self-assembly and hydrogelation of an amyloid peptide fragment. *Biochemistry* **2008**, *47*, 4597–4605. [[CrossRef](#)] [[PubMed](#)]
55. Williams, R.J.; Smith, A.M.; Collins, R.; Hodson, N.; Das, A.K.; Ulijn, R.V. Enzyme-assisted self-assembly under thermodynamic control. *Nat. Nanotechnol.* **2009**, *4*, 19–24. [[CrossRef](#)] [[PubMed](#)]
56. Vigier-Carrière, C.; Boulmedais, F.; Schaaf, P.; Jierry, L. Surface-Assisted Self-Assembly Strategies Leading to Supramolecular Hydrogels. *Angew. Chem. -Int. Ed.* **2018**, *57*, 1448–1456. [[CrossRef](#)]
57. Criado-Gonzalez, M.; Iqbal, M.H.; Carvalho, A.; Schmutz, M.; Jierry, L.; Schaaf, P.; Boulmedais, F. Surface Triggered Self-Assembly of Fmoc-Tripeptide as an Antibacterial Coating. *Front. Bioeng. Biotechnol.* **2020**, *8*, 938. [[CrossRef](#)] [[PubMed](#)]
58. Chen, J.; Zou, X. Self-assemble peptide biomaterials and their biomedical applications. *Bioact. Mater.* **2019**, *4*, 120–131. [[CrossRef](#)]
59. Li, J.; Du, X.; Hashim, S.; Shy, A.; Xu, B. Aromatic-aromatic interactions enable α -helix to β -sheet transition of peptides to form supramolecular hydrogels. *J. Am. Chem. Soc.* **2017**, *139*, 71–74. [[CrossRef](#)]
60. Diaferia, C.; Rosa, E.; Accardo, A.; Morelli, G. Peptide-based hydrogels as delivery systems for doxorubicin. *J. Pept. Sci.* **2021**, *28*, e3301. [[CrossRef](#)]
61. Gallo, E.; Diaferia, C.; Rosa, E.; Smaldone, G.; Morelli, G.; Accardo, A. Peptide-based hydrogels and nanogels for delivery of doxorubicin. *Int. J. Nanomed.* **2021**, *16*, 1617–1630. [[CrossRef](#)] [[PubMed](#)]
62. Sun, Y.; Kang, C.; Liu, F.; Zhou, Y.; Luo, L.; Qiao, H. RGD Peptide-Based Target Drug Delivery of Doxorubicin Nanomedicine. *Drug Dev. Res.* **2017**, *78*, 283–291. [[CrossRef](#)] [[PubMed](#)]

63. Thota, C.K.; Yadav, N.; Chauhan, V.S. A novel highly stable and injectable hydrogel based on a conformationally restricted ultrashort peptide. *Sci. Rep.* **2016**, *6*, 31167. [[CrossRef](#)] [[PubMed](#)]
64. Alam, S.; Panda, J.J.; Mukherjee, T.K.; Chauhan, V.S. Short peptide based nanotubes capable of effective curcumin delivery for treating drug resistant malaria. *J. Nanobiotechnol.* **2016**, *14*, 26. [[CrossRef](#)] [[PubMed](#)]
65. Altunbas, A.; Lee, S.J.; Rajasekaran, S.A.; Schneider, J.P.; Pochan, D.J. Encapsulation of curcumin in self-assembling peptide hydrogels as injectable drug delivery vehicles. *Biomaterials* **2011**, *32*, 5906–5914. [[CrossRef](#)]
66. Baek, K.; Noblett, A.D.; Ren, P.; Suggs, L.J. Self-assembled nucleo-tripeptide hydrogels provide local and sustained doxorubicin release. *Biomater. Sci.* **2020**, *8*, 3130–3137. [[CrossRef](#)] [[PubMed](#)]